Journal Pre-proof

Use of light response curve parameters to estimate gross primary production capacity from chlorophyll indices of global observation satellite and flux data

Kanako Muramatsu, Emi Yoneda, Noriko Soyama, Ana López-Ballesteros, Juthasinee Thanyapraneedkul

Please cite this article as: Muramatsu, K., Yoneda, E., Soyama, N., López-Ballesteros, A., Thanyapraneedkul, J., Use of light response curve parameters to estimate gross primary production capacity from chlorophyll indices of global observation satellite and flux data, *Science of Remote Sensing*, https://doi.org/10.1016/j.srs.2024.100164.

This is a PDF file of an article that has undergone enhancements after acceptance, such as the addition of a cover page and metadata, and formatting for readability, but it is not yet the definitive version of record. This version will undergo additional copyediting, typesetting and review before it is published in its final form, but we are providing this version to give early visibility of the article. Please note that, during the production process, errors may be discovered which could affect the content, and all legal disclaimers that apply to the journal pertain.

1   **Use of light response curve parameters to estimate gross primary production**

2   **capacity from chlorophyll indices of global observation satellite and flux data**

3

4   Kanako Muramatsu[1,2*] Emi Yoneda[2], Noriko Soyama[3], Ana López-Ballesteros[4],

5   Juthasinee Thanyapraneedkul[5]

6   [1] Department of Chemistry, Biology, and Environmental Science, Faculty of Science,

7   Nara Women's University, Kitauoyanishi-machi, Nara 630-8506, Japan

8   [2] Department of Information and Computer Sciences, Graduate School of Science, Nara

9   Women's University, Kitauoyanishi-machi, Nara, 630-8506, Japan

10   [3] Faculty of Human Studies, Tenri University, 1050, Somanouchi, Tenri, Nara 632-8510,

11   Japan

12   [4] Department of Agricultural and Forest Systems and the Environment, Agrifood

13   Research and Technology Centre of Aragon (CITA), Avda. Montañana 930, 50059

14   Zaragoza, Spain

15   [5] Department of Environmental Science, Faculty of Science and Technology, Thammasat

16   University, Pathumthani Province, 12120, Thailand.

17

18   **Abstract**

19   The photosynthetic rate has a nonlinear relationship with PAR during the day. We

20   previously developed an algorithm for estimating GPP capacity, which is defined GPP

21   under low-stress condition, using light response curves (LRCs). In this study, we studied

22   the characteristics of LRC parameters of the initial slope and the maximum gross

23   photosynthesis rate (P_{max}), and formulas to calculate P_{max} from the relationship between

24   the chlorophyll index of the green and near-infrared (NIR) bands (CI_{green}) and the GPP

25 capacity at PAR = 2000 μmol m^{-2} s^{-1} (GP2000) for nine vegetation types spanning

26 tropical to subarctic climates on the Eurasian and North American continents using eddy

27 covariance flux measurements and Moderate Resolution Imaging Spectrometer (MODIS)

28 data. The slope of the relationship between CI$_{green}$ and GP2000 was highest for sites

29 dominated by herbaceous plants such as open shrubland, savanna, and cropland (rice

30 paddy); it was lower at sites dominated by woody plants. The yearly GPP/GPP capacity

31 ratio was close to one in flux data. When the method was applied to satellite data, the

32 daily GPP capacity exhibited a similar seasonal pattern to that of the Flux GPP and

33 MODIS GPP products. Under high dryness conditions, Flux GPP showed the drop from

34 the GPP capacity estimated from CI$_{green}$ and diurnal PAR data around noon, and they were

35 nearly identical during the early morning and late afternoon. The instantaneous GPP

36 capacity could be considered the baseline of the instantaneous GPP with stress-free

37 conditions and important for quantifying midday depression at the sub-day scale.

38

39 **Keywords**

40 CI$_{green}$; eddy covariance flux; GPP; light response curve; MODIS; rectangular hyperbola

41 equation

42

43 **1. Introduction**

44 Accurate observations of CO_2 exchange between the canopies of different types of plants

45 and the atmosphere are crucial for understanding the carbon cycle and land–atmosphere

46 feedback processes in climate change scenarios. Gross primary production (GPP), which

47 represents the total amount of CO_2 absorbed by plants through photosynthesis, accounts

48 for the largest global carbon flux (Beer *et al.*, 2010). Satellite remote sensing (e.g., the

49 Earth Observing System) can monitor vegetation phenology globally and has been used

50 to estimate GPP using models based on light use efficiency (LUE) (Monteith, 1972;

51 Heinsch *et al.*, 2006). Such models assume a linear relationship between GPP and

52 photosynthetically active radiation (PAR), with the incorporation of LUE (ϵ) as a

53 coefficient as follows:

$$\text{GPP} = \epsilon f_{\text{APAR\_canopy}} \text{PAR} \tag{1}$$

55 where $f_{\text{APAR\_canopy}}$ is the fraction of PAR absorbed by the plant canopy, which is estimated

56 from the normalized vegetation index (NDVI) (Myneni *et al.*, 1994; Rouse *et al.*, 1973)

57 or from the inversion of the three-dimensional radiation transfer of surface reflectance in

58 vegetation canopies (Myneni *et al.*, 2002). This parameter is significantly affected by non-

59 photosynthetic canopy components such as stems and litter (Asner *et al.*, 1998). When

60 estimating GPP, photosynthetically active vegetation (mostly green leaves) should be

61 distinguished from non-photosynthetically active vegetation (Xiao et al., 2004a,b). Xiao

62 *et al.* developed a vegetation photosynthesis model (VPM) using the fraction of APAR

63 attributable to photosynthetically active vegetation ($f_{\text{APAR\_PAV}}$) in plant canopies. The

64 parameter is estimated using the enhanced vegetation index (EVI) (Huete *et al.*, 1997)

65 because the seasonal dynamics of EVI agree well with the observed GPP of temperate

66 deciduous broadleaf forests and boreal–northern evergreen needleleaf forests during the

67 growing season (Xiao *et al.*, 2004 a, b).

68

69 GPP estimation models that focus on chlorophyll have been proposed based on a concept

70 similar to the LUE-based model. For boreal forests, chlorophyll-absorbed PAR (APAR_{chl})

71 is strongly related to gross ecosystem production flux, whereas canopy-absorbed PAR

72 (APAR_{canopy}) is only weakly related, as revealed by Moderate Resolution Imaging

73   Spectrometer (MODIS) observations (Zhang *et al.*, 2009). For deciduous broadleaf

74   forests, the Medium Resolution Image Spectrometer (MERIS) terrestrial chlorophyll

75   index (MTCI) (Dash *et al.*, 2004, 2007, 2010) is strongly correlated with daily GPP based

76   on flux observations. The EVI from MODIS is also strongly correlated with GPP.

77   Differences between the MTCI and EVI indices are apparent in time series in which there

78   is a greater time lag between the onset of the depression in GPP at the end of season and

79   a downturn in the EVI (Harris *et al.*, 2010). For crops (Gitelson *et al.*, 2006; Peng *et al.*,

80   2012) and mixed temperate forests (Croft *et al.*, 2015), midday GPP has a strong linear

81   relationship with the total chlorophyll content in the canopy multiplied by the PAR.

82

83   The photosynthetic rate is not linearly related to PAR at the leaf scale and often not at the

84   canopy scale. To include this nonlinearity in GPP estimation models, light-response

85   curves (LRCs) of the GPP and PAR relationship have been used (Furumi *et al.*, 2005;

86   Harazono *et al.*, 2009; Ide *et al.*, 2010). The maximum gross photosynthesis rate (P_{max})

87   in the GPP–PAR curve is determined from the relationship between the vegetation index

88   and observed GPP. During the midday period, the photosynthetic rate often decreases due

89   to stomatal closure in dry weather conditions (Pathre *et al.*, 1998; Pessarakli *et al.*, 2005),

90   and this is not related to chlorophyll content in leaves. These levels are related to the light

91   reactions involved in photosynthesis, and stomatal opening and closure is related to the

92   carbon reduction cycle. Thus, the estimation of GPP can be separated according to these

93   two phenomena (Thanyapraneedkul *et al.*, 2012). Here, we focus on the former, and

94   defined the GPP capacity as GPP under low-stress conditions. To estimate this capacity,

95   we use a GPP capacity–PAR, which estimates the relationship in the form of a rectangular

96   hyperbola. It is assumed that the P_{max} at light saturation under low-stress conditions is

97 mainly dependent on the total chlorophyll content in a canopy. We replace this with the

98 GPP capacity at a PAR that is sufficiently high at 2000 µmol m^{-2} s^{-1} (hereafter, GP2000).

99 This has a linear relationship with the chlorophyll index (CI) of the green and near-

100 infrared band (CI$_{green}$), which is strongly correlated with chlorophyll content (Gitelson *et*

101 *al.*, 2006; Thanyapraneedkul *et al.*, 2012). It is a close proxy of plant absorption

102 coefficients in the green spectral region (Gitelson *et al.*, 2019).

103

104 The advantage of a model using the GPP capacity–PAR curve is that the diurnal variation

105 in the GPP capacity can be calculated, as shown in Fig. 1. This GPP capacity is considered

106 the baseline, which is the GPP under unstressed conditions. The midday depression is the

107 area between the baseline and the GPP (Muramatsu, 2018). We have previously examined

108 the parameters of the GPP capacity curve in North America, Japan, and Thailand, for the

109 following types of vegetation cover recognized by the International Geosphere Biosphere

110 Program (IGBP): open shrubland, savanna, grassland, cropland (rice paddy), closed

111 shrubland (permanent wetland), deciduous needleleaf forest, evergreen needleleaf forest,

112 and evergreen broadleaf forest (Thanyapraneedkul *et al.*, 2012; Mineshita *et al.*, 2016;

113 Muramatsu *et al.*, 2017). Plants in Europe, including Siberia, belonging to subarctic

114 climate regions, have not yet been analyzed and should be evaluated to ascertain whether

115 the rules governing the parameters of plant functional types differ among continents with

116 subarctic to tropical climates. It is unclear whether the parameters and relationship

117 between GP2000 and CI$_{green}$ vary among vegetation types. Thus, in this study, we

118 examined these characteristics among different vegetation types and examined the daily

119 and diurnal variation in GPP capacity estimated from MODIS CI$_{green}$ in comparison with

120 MODIS GPP and Flux GPP.
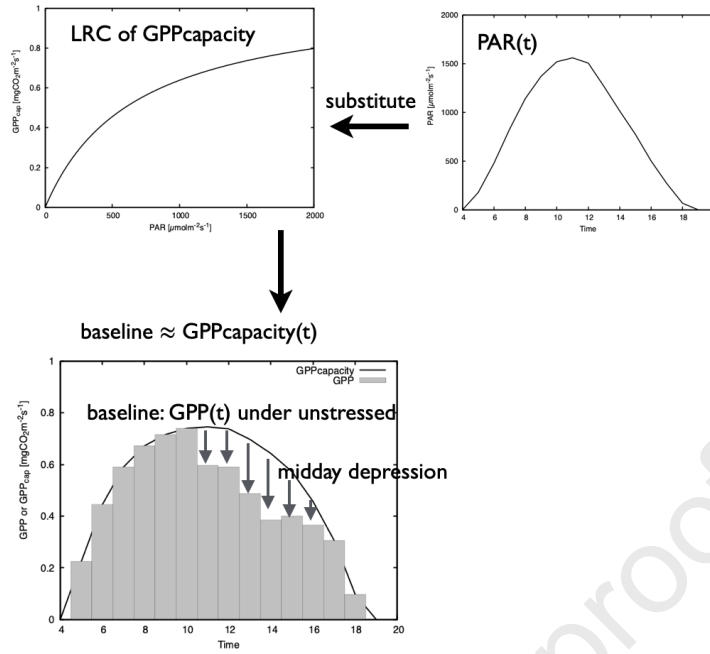
121

122 Figure 1. Diurnal variation in instantaneous GPP capacity can be calculated from light response curve of

123 GPP capacity and diurnal variation in photosynthetically active radiation (PAR). Baseline is defined as

124 GPP under unstressed conditions, and GPP capacity is considered the baseline for midday depression.

125

126 **2. Data and Methods**

127 *2.1. Background: LRC formula*

128 We used an LRC for canopy GPP capacity (Thanyapraneedkul *et al.*, 2012), as follows:

129 $$\text{GPP}_{\text{capacity}}\big(\text{PAR}(t)\big) = \frac{\alpha P_{\max} \text{PAR}(t)}{1 + \alpha \text{PAR}(t)} \qquad (2)$$

130 where α (m^2 s (μmol photon)$^{-1}$) is a parameter related to the initial slope, $P_{\max}$ (mgCO$_2$

131 m^{-2} s^{-1}) is considered the maximum rate of canopy gross photosynthesis at light

132 saturation, $\alpha P_{\max}$ is the initial slope of the LRC and represents the apparent quantum

133 efficiency under weak light conditions. GP2000, already described above (Fig. 2), can be

134 estimated (Thanyapraneedkul *et al.*, 2012; Mineshita *et al.*, 2016; Muramatsu *et al.*, 2017)

135 using the green CI (CI$_{\text{green}}$) (Gitelson *et al.*, 2006) based on satellite reflectance data in

136 the near infrared (R$_{\text{NIR}}$) and green (R$_{\text{green}}$) bands as follows:

137 $$GP2000 = aCI_{green} + b \qquad (3)$$

138 $$CI_{green} = \frac{R_{NIR}}{R_{green}} - 1 \qquad (4)$$

139

140 Another rectangular hyperbola LRC formula is often used:

141 $$GPP\big(PAR(t)\big) = \frac{QP_{max}PAR(t)}{P_{max} + QPAR(t)} \qquad (5)$$

142 where Q is the apparent quantum efficiency and is the initial slope of the LRC; P_{max} is

143 the maximum rate of GPP. Equations (2) and (5) are the same when the relationship

144 between the parameters in both formulas is $\alpha = Q/P_{max}$. We used a rectangular
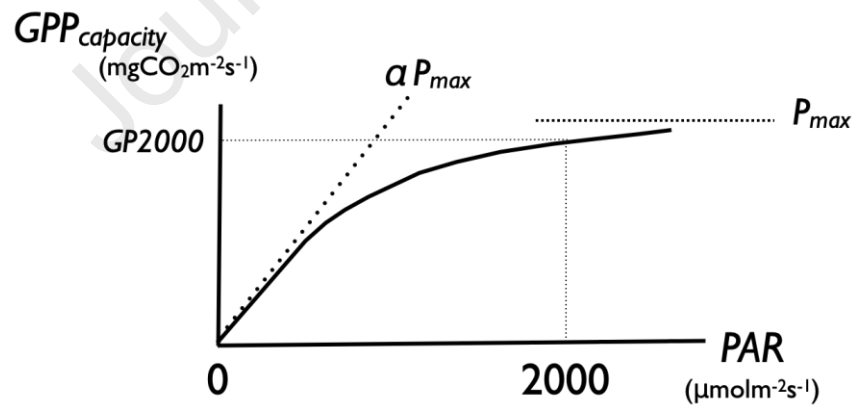
145 hyperbola equation to reduce the number of parameters. Owen *et al.* (2007) showed that

146 when the theoretical maximum CO_2 uptake capacity at a high light intensity of 2000

147 (μmol m^{-2} s^{-1}) is expressed as a rectangular hyperbola, the value is similar to that

148 obtained from a non-rectangular hyperbola equation.

149

150

151 Figure 2. Light response curve of gross primary production capacity (GPP capacity).

152

153 Table 1. Flux site descriptions: IGBP class; OSH: Open shrubland, SAV: Savanna, GRA: Grassland, CRO: Cropland, DBF: Deciduous broadleaf forest, CSH: Closed shrubland, WET:

154 Permanent wetland, DNF: Deciduous needleleaf forest, ENF: Evergreen needleleaf forest, EBF: Evergreen broadleaf forest. The symbol * in site ID shows newly added data; and the

155 symbols ⬦, ∘ and ♯ shows previous study data in Thanyapraneedkul et al. (2012), Mineshita et al. (2016), and Muramatsu etal. (2017), respectively.

IGBP class	Site ID (This	Data year	Name and Country	Location	Annual temp. ($^{\circ}$C)	Annual precip.(mm)	Dominant Species	Canopy height(m)	Reference
OSH	ES-Agu*	2007	Balsa Blanca, Spain	36.9406˚N 2.0329˚W	18.0	220	*Machrocloa tenacissima*	1	(López-Ballesteros et al., 2016 López-Ballesteros et al., 2018)
OSH	US-Ses∘	2007	Sevilleta shrubland, USA	34.3349˚N 106.7442˚W	13.7	273	*Larrea tridentata, Bouteloua eriopoda*	0.75	(Anderson-Teixeira et al., 2011)
SAV	US-Wjs∘	2007	Willard Juniper, Savannah, USA	34.4255˚N 105.862˚W	15.2	361	*Juniperus monosperma, Bouteloua gracilis*	2	(Anderson-Teixeira et al., 2011)
GRA	CA-Let⬦	2003	Alberta-Mixed Grass, Prairie, Canada	49.709˚N 112.940˚W	5.4	398	*Agropyron dasystachyum A. smithii*	0.317 ± 0.074 (2001-2006)	(Flanagan et al., 2011)
CRO	JP-MSE♯	2001-2004	Mase paddy, Japan	36.054˚N 136.054˚E	13.7	1200	rice (*Oryza sativa*)	1.2 (max.)	(Ono et al., 2013)
DBF	FR-Hes*	2007	Hess, France	48.6742˚N 7.0656˚E	9.2	820	Beech (*Fagus sylvatica L.*)	13	(Granier et al., 2008)
DBF	JP-TKY⬦	2003	Takayama, Japan	36.146˚N 37.423˚E	6.4	2293.5	*Betula ermanii Quercus crispula*	15-20	(Saigusa et al., 2002) (Hirata, et al., 2008)
CSH (WET)	US-Los*	2007	Lost Creek, USA	46.0827˚N 89.9792˚W	4.1	828	Alder (*Alnus incana*) Willow (*Salix*)	2	(US-Los; Sulman et al., 2009)
DNF	RU-YLF*	2004-2007	Spasskaya Pad, Yakutsk, Russia	62.255˚N 129.241389 *E	-10.0 (1961-1990)	236.9 (1961-1990)	Dahurica larch (*Larix cajanderi*)	18	(Ohta et al., 2008)
DNF	JP-TMK⬦	2003	Tomakomai, Japan	42.737˚N 141.519˚E	6.2	1043	Japanese larch (*Larix kaempferi*)	15	(Hirata, et al., 2007, 2008)
ENF	NL-Loo*	2007	Loobos, Netherlands	52.1679˚N 5.7440˚E	9.8	786	Scots pine (*Pinus sylverstris*)	15.1 (1977)	(Dolman et al., 2002)
ENF	IT-Lav*	2007	Lavarone, Italy	45.9553˚N 11.2812˚E	7.0	1150	Fir *Abies alba* (70%)	33-36	(Marcolla et al., 2003)
ENF	RU-YPF*	2004-2007	Spasskaya Pad, Yakutsk, Russia	62.241389˚N 129.650556˚E	-10.0 (1961-1990)	236.9 (1961-1990)	Pine (*Pinus sylvestris*)	10	(Matsumoto et al., 2008)
ENF	JP-FJY⬦	2003	Fujiyoshida, Japan	35.454˚N 138.762˚E	10.1	1483	Japanese red pine (*Pinus densiflora*)	20	(Mizoguchi et al., 2012) (Hirata, et al., 2008)
EBF	FR-Pue*	2007	Puechabon, France	43.7414˚N 3.5958˚E	10.4	1230	Holm oak (*Quercus ilex L.*)	6	(Soudani et al., 2014)
EBF	TH-SHR⬦	2003	Sakaerat, Thailand	14.492˚N 101.916˚E	24.1	1200-1300	*Hopea ferrea pierre*	35	(Aguilos et al., 2007) (Hirata, et al., 2008)

156   ***2.2. Data collection sites for different IGBP classes and fluxes***

157   Flux data were obtained for nine IGBP vegetation classes (Steffen *et al.*, 1992). Table 1

158   lists the collection sites. Flux data from Europe (http://www.europe-fluxdata.eu/home)

159   and Siberia Asia (http://www.asiaflux.net) were used to determine the LRC parameters.

160   For the European sites (ES-Agu, FR-Hes, NL-Loo, IT-Lav, and FR-Pue), GPP and vapor

161   pressure deficit (VPD) data were extracted from level 4 products and PAR data were

162   extracted from level 2 products, with a 30 min interval, in 2007. GPP in Siberia was

163   calculated from net ecosystem exchange (NEE) and air temperature data, with a 30 min

164   interval, from 2004 to 2007. Details of the GPP calculation are provided in Appendix A.

165   The processing of flux data from the United States (US-Ses, US-Wjs, and US-Los),

166   Canada (CA-Let), Japan (JP-TKY, JP-TMK, and JP-MSE), and Thailand (TH-SKR) and

167   the LRC parameters used in this study are described in Thanyapraneedkul *et al*. (2012) ,

168   Mineshita *et al.* (2016), and Muramatsu *et al.* (2017).

169

170   *2.2.1. Satellite data*

171   To determine the relationships between the LRC parameters and vegetation indices,

172   MODIS surface reflectance data (MOD09A1) for the same year as the flux data were

173   obtained from the MODIS Land Products Subsets project website (ORNL DAAC, 2008).

174   Data for the period of 2000–2015 were used to determine the selection criteria for pure

175   pixels. The MOD09A1 product has a spatial resolution of 500 m every 8 days, with

176   correction for the effects of scattering and absorption by atmospheric components and

177   aerosols using the transmission, reflectance, and spherical albedo of gas molecules and

178   aerosols (Vermote *et al.*, 2002). The MODIS bands used in this study are shown in Table

179   2.

180   Table 2. MODIS bands and bandwidths used in this study

Band	Bandwidth (nm)	Notation in this study
3	459–479	blue
4	545–565	red
1	620–670	green
2	841–876	NIR
5	1230–1250	1.2 µm

181

182 The MODIS GPP product (MOD17A2H) (Running *et al.*, 2015) data for newly added

183 flux sites (ES-Agu, FR-Hes, RU-YLF, NL-Loo, IT-Lav, RU-YPF, and FR-Pue) were

184 obtained for the same time period. This product has a spatial resolution of 500 m every 8

185 days and the data are expressed in units of kg C m^{-2}.

186

187 ***2.3. Data preprocessing for the newly added GHG-Europe and Siberia flux sites***

188 *2.3.1. Selection of clear and pure MODIS pixels for vegetation index calculation and*

189 *CI$_{green}$ calculation at flux sites*

190 MODIS data from 2000 to 2015 for GHG-Europe sites were used to determine the criteria

191 for selecting clear and pure pixels in the MODIS reflectance data. Four pixels from

192 different positions at each site were examined. Because of the uniformity of the land

193 cover, it was considered acceptable to use only four pixels in this study, despite nine

194 pixels (one pixel corresponding to the site position, and eight pixels surrounding the

195 center pixel) having been used in a previous study of a paddy site (Muramatsu *et al.*,

196 2017). To minimize the effects of clouds, cloud shadows, and aerosols, surface

197 reflectance data were used with MOD35 cloud regions recorded as 00, cloud shadows as

198 0, aerosol amounts as 00 and 01, and cirrus as 00. However, some contamination

199 remained in the form of thin clouds. To select clear and pure pixels, we used satellite data

200 with blue and 1.2 µm reflectance, and the band ratio of the blue and red reflectance within

201 three standard deviations of the 16-year mean (Table 3), in accordance with Muramatsu

202 *et al.* (2017).

203

204 Table 3. Spectral reflectance (R) in the blue and 1.2 µm bands, and ratio of blue and red reflectance.

Spectral reflectance or band ratio	Mean	Standard deviation
R_{blue}	0.041	0.013
$R_{1.2\mu m}$	0.218	0.067
R_{blue}/R_{red}	0.505	0.053

205

206 CI_{green} was calculated every 16 days from the reflectance of a pixel corresponding to the

207 flux site location. If the data were available every 8 days, the average of two values was

208 used. If only one value was available for 16 days, that value was used. If no data were

209 available for 16 days because the selection criteria for clear and pure pixels were not met,

210 that day was treated as missing data.

211

212 *2.3.2. Selection of GPP under low-stress VPD conditions*

213 A high VPD causes a decrease in the rate of photosynthesis during the day (Pathre *et al.*,

214 1998; Thanyapraneedkul *et al.*, 2012; Mineshita *et al.*, 2016). In this study, low-stress

215 GPP data corresponding to the period before and after the midday depression of GPP were

216 selected. To determine the threshold for VPD, diurnal variation in GPP, PAR, and VPD

217 was examined every 30 min, and the VPD value at the start of the diurnal depression in

218 GPP was used as the threshold value. Data every 30 min with VPD values lower than the

219 VPD threshold were selected to determine the parameters of the LRC for GPP capacity.

220   In previous studies (Thanyapraneedkul *et al.*, 2012; Mineshita *et al.*, 2016; Muramatsu *et*

221   *al.*, 2017), the VPD threshold was determined to be 1.5 (kPa) for open shrubland (US-

222   Ses) and savanna (US-Wjs), and 2.0 (kPa) for grassland (CA-Let), rice paddy (JP-MSE),

223   wetland (US-Los), deciduous broadleaf forest (JP-TKY), evergreen needleleaf forest (JP-

224   FJY), and evergreen broadleaf forest (TH-SKR). For the GHG-Europe flux sites and

225   Siberia flux sites, it was 0.8 for open shrubland (ES-Agu) and 1.5 (kPa) for the others.

226   Although it is ideal to use a unified VPD threshold for all sites, the conditions under which

227   a decrease in GPP occurred without a decrease in PAR differed among vegetation types.

228

229   *2.3.3. Parameters of the LRC for the GPP capacity estimation algorithm of the GHG-*

230   *Europe and Siberia flux sites*

231   To determine the two parameters α and P_{max} in Equation (2), flux data were first fitted to

232   Equation (2) for every 16-day period using a least-squares method, which corresponded

233   to the MODIS satellite observations. Then, α values with a fitting error of less than 35%

234   were averaged (α_{ave}), corresponding to the data during the growing season. Second,

235   Equation (2) was re-fitted using α_{ave} to determine P_{max} for each 16-day period. Third,

236   GP2000 for each 16-day period was calculated by substituting PAR = 2000 (μmol m^{-2} s^{-}

237   ^{1}), α_{ave}, and P_{max} into Equation (2). To characterize the differences in LRC parameters,

238   α_{ave}, seasonal changes in P_{max}, and the seasonal value ranges in $\alpha_{ave}P_{max}$ were compared

239   for various vegetation types using the results from the newly added data and data from

240   previous studies (Table 1).

241

242 ***2.4. Comparison of the relationship between GP2000 and CI$_{green}$ for various***

243 ***vegetation types***

244 The relationship between CI$_{green}$ from MODIS and GP2000 for various vegetation types

245 were compared using the results from the flux sites listed in Table 1, and the relationship

246 in Equation (3) was determined for every vegetation type. Next, the linear relationship in

247 Equation (3) for the newly added data was evaluated using a cross-validation method.

248 The flux data were divided into two groups to include seasonal changes equally. Flux data

249 were sequentially numbered every 16 days corresponding to the MODIS observation

250 dates, and the sequential number was divided by 2 for Group 1 if the remainder was 0 and

251 Group 2 if the remainder was 1. For Group 1 and 2, the α$_{ave}$ and P$_{max}$ of the LRCs for

252 every 16-day period were calculated using flux data, GP2000 was calculated from an

253 LRC with the calculated parameters, and the relationship between MODIS CI$_{green}$ and

254 GP2000 was determined. The CI$_{green}$ value of one group (Group1/2) was substituted into

255 the relationship between the other group (Group 2/1). For the evergreen needleleaf forest

256 at NL-Loo, IT-Lav, and RU-YPF, NL-Loo and IT-Lav were divided into two data groups

257 using the remaining sequential numbers, while RU-YPF was divided into two data

258 groups, one for 2004 and 2006 and the other for 2005 and 2007.

259

260 ***2.5. Comparison of the GPP/GPP capacity ratio at the canopy level for various***

261 ***vegetation types***

262 Next, the GPP capacity at the canopy level was calculated using the LRCs. The seasonal

263 variation in the GPP/GPP capacity ratio, and the annual value of the ratio, i.e., the ratio

264 between the annual GPP and the annual GPP capacity at the canopy level were compared

265 for various vegetation types using the results from the GHG-Europe, Ameri-Flux, and

266   AsiaFlux sites.

267

268   *2.6. Daily and diurnal variation in GPP capacity from MODIS CI_{green} for newly added*

269   *flux sites*

270   Daily and diurnal variation in GPP capacity at the satellite level were calculated using

271   Equation (2) for the newly added flux sites. After estimating GP2000 from MODI CI_{green},

272   P_{max} was calculated as follows:

273    $$P_{max} = (GP2000 \times (1 + \alpha_{ave} \times 2000))/(\alpha_{ave} \times 2000). \tag{5}$$

274   Then the estimated GPP capacity values from CI_{green} were compared to the Flux GPP and

275   MODIS GPP products.

276

277   **3. Results**

278   *3.1. LRC parameters of GPP capacity*

279   The LRC parameters of α_{ave} in Equation (2) for all data in Table 1 are shown in Fig. 3.

280   The values ranged from 0.0006 to 0.0046, with no clearly characteristic values applicable

281   to every vegetation type. The standard deviation was largest at the Russian site. The P_{max}

282   values every 16 days exhibited seasonal changes as shown in Fig. 4. These differed for

283   open shrub and savanna. At the Es-Agu site, a maximum value of approximately 0.3 was

284   obtained in winter, with low values in summer, which is a dry season with high

285   temperatures. Clear seasonal changes in P_{max} were observed in herbaceous plants in

286   grassland, rice paddy, closed shrubland (permanent wetland), and deciduous broadleaf

287   forests, with maximum values of 1, 2.4, 1.1, and 1.6, respectively. Seasonal changes were

288   also observed in deciduous needleleaf forests. The dominant species at both sites was

289   larch, but the maximum values differed between Japan (JP-TMK) and Siberia (RU-YLF).

290   The maximum value was highest (∼2.5) at JP-TMK. In evergreen needleleaf forests, P_{max}

291   exhibited slight seasonal changes, except at JP-FJY. The *Pinus densiflora* forests at JP-

292   FJY exhibited clear seasonal changes, with a change in leaf color from green to yellow

293   evident in photographs taken on October 11 and 31 October 2007, respectively. In

294   evergreen broadleaf forests, the maximum values were lower in Europe (FR-Pue) than in

295   tropical areas (TH-SKR). Seasonal values of P_{max} could be converted into GP2000 by

296   substituting $PAR(t) = 2000$ into Equation (2), and the seasonal changes in GP2000 are

297   shown in Appendix B.

298

299   Figure 5 shows the average and the range of seasonal changes in terms of the minimum

300   and maximum values during the growing season from the initial slope of the LRC in

301   Equation (2) of $\alpha_{ave}P_{max}$. The average values were 0.0003–0.002. The smallest values

302   were for open shrubland and savanna, followed by grass and cropland (rice paddy). For

303   closed shrubland (in a permanent wetland), deciduous broadleaf, deciduous needleleaf,

304   evergreen needleleaf, and evergreen broadleaf forests, the average values were 0.001–

305   0.002; the highest value recorded was in deciduous broadleaf forest, which also had the

306   largest range of seasonal change. Evergreen forests also displayed seasonal changes in

307   the initial slope, with particularly large changes in the *P. densiflora* forests at the JP-FJY
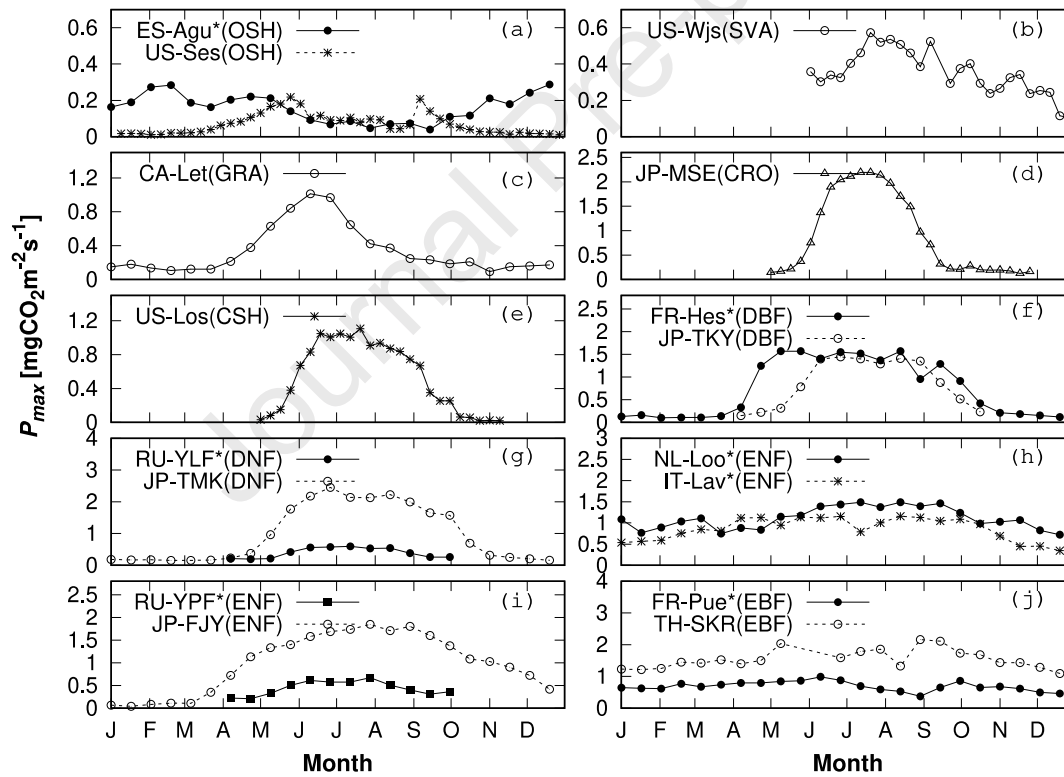
308   site.
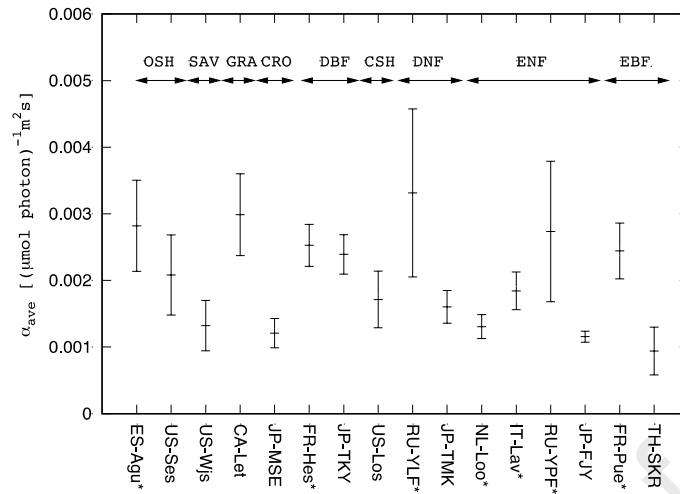
309

310   Figure 3. Mean and standard deviation of the GPP capacity LRC parameters for α_{ave} at 16 sites.

311

312

313   Figure 4. Seasonal changes in P_{max} for (a) open shrubland (OSH), (b) savanna (SVA), (c) grassland

314   (GRA) (d) cropland (CRO) rice paddy, average value over 4 years, (e) deciduous broadleaf forest (DBF),
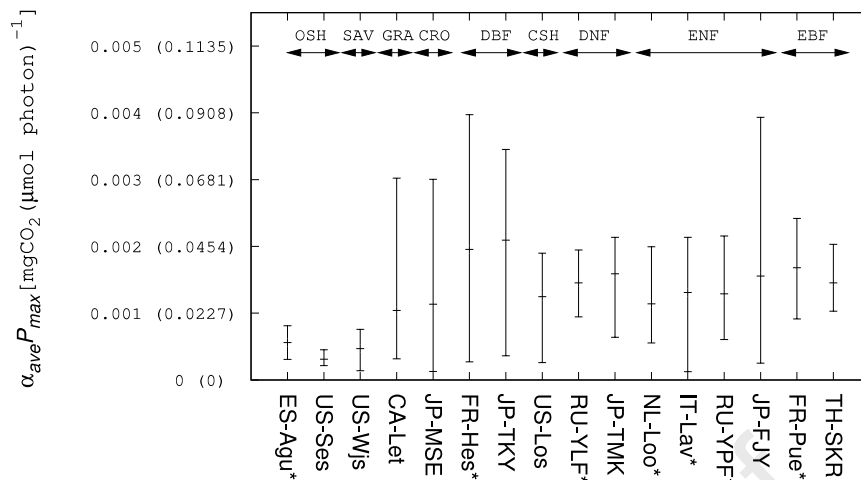
315   (f) closed shrubland (CSH) in a permanent wetland, (g) deciduous needleleaf forest (DNF), RU-YLF,

316   average value over 4 years, (h, i) evergreen needleleaf forest (ENF), RU-YPF, average value over 4 years,

317   and (j) evergreen broadleaf forest (EBF).

318

Figure 5. Average and seasonal range of initial slope of the LRC at 16 sites. The $\alpha_{ave}P_{max}$ value is shown

in $mgCO_2$ (μmol photon)$^{-1}$. The value converted into $molCO_2$ (mol photon)$^{-1}$, which is frequently used in

the field of plant physiology, is shown in parentheses on the vertical axis.

322

3.2. Relationship between CI_{green} and GP2000

The relationship between CI_{green} and GP2000 was investigated for newly added data and

data from previous studies for various vegetation types. The data are summarized in Table

4 and illustrated in Fig. 6. For open shrubland, savanna, grassland, and cropland (rice

paddy), the data displayed a linear relationship. The newly added ES-Agu site data were

also distributed near the regression line. For deciduous broadleaf forests and permanent

wetland there was a linear relationship. Deciduous broadleaf *Fagus sylvatica* forests in

France (FR-Hes) and *Betula ermanii* and *Quercus crispula* forests in Japan (JP-TKY)

exhibited a similar distribution of hysteresis. The slope was lower for DBF and CSH (Fig.

6(b)) than for OSH, GRS, and CRO (Fig. 6(a)). The US-Los site was in closed shrubland

(permanent wetland) and had a different vegetation type. Nevertheless, the relationship

between CI_{green} and GP2000 at this site was similar to that of deciduous broadleaf forests.

This site had seasonal variation in GP2000 and P_{max}, but the degree of variation was less

than that in broadleaf forests. These characteristics were also observed in the relationship

337   between CI_{green} and GP2000. In the *P. densiflora* forests of JP-FJY, there were 4-fold (2–

338   6-fold) seasonal changes in CI_{green} over 1 year due to the change in leaf color, which was

339   recorded as described in the previous section. The slope of the relationship was the same

340   as that for deciduous broadleaf forests. The range of CI_{green} values at the NL-Loo and RU-

341   YPF sites were lower than that at JP-FJY. Mixed forests in which evergreen needleleaf

342   trees accounted for more than 70%, such as those at IT-Lav, had a range of CI_{green} values

343   similar to those observed at JP-FJY, but the data points were widely distributed. For the

344   evergreen broadleaf forests, the magnitudes of changes in CI_{green} and GP2000 over 1 year

345   were small at 2- and 0.5-fold, respectively. Although there was no relationship between

346   CI_{green} and GP2000 at each site, the slope of the linear regression for the relationship

347   between the two sites was the same as that between deciduous broadleaf forest and

348   evergreen needleleaf forest within a small range of error.

349

350   The highest slope value (0.40) was obtained for open shrubland, savanna, and cropland

351   (rice paddy). The next highest value was obtained for deciduous needleleaf forest (0.24),

352   and similar slopes in the range of 0.15–0.18 were obtained for the other vegetation types,

353   i.e., deciduous broadleaf forest, closed shrubland, evergreen needleleaf forest, and

354   evergreen broadleaf forest. The intercept of Equation (3) tended to have a negative value

355   for deciduous vegetation types and a value close to zero for evergreen vegetation types.
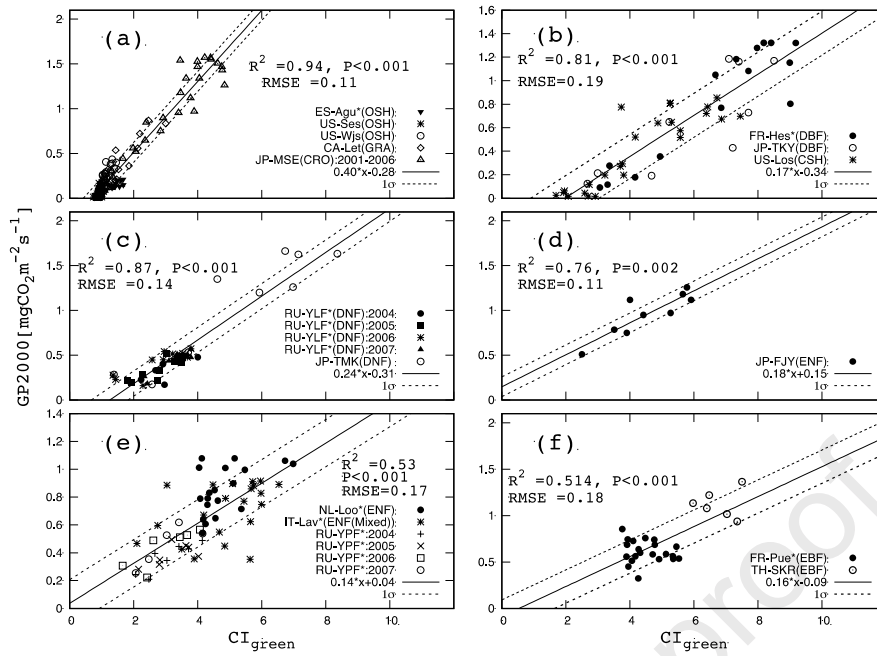
356

357 Figure 6. Relationship between CI_{green} and GP2000 for (a) open shrubland (OSH), savanna (SAV),

358 grassland (GRA), and cropland (CRO) rice paddy (JP-MSE), (b) deciduous broadleaf forest (DBF)

359 and closed shrubland (CSH) in a permanent wetland, (c) deciduous needleleaf forest (DNF), (d)

360 evergreen needleleaf forest (ENF) of *Pinus densiflora* in JP-FJY, (e) ENF except JP-FJY, and (f)

361 evergreen broadleaf forest (EBF). Solid and dashed lines represent linear regression fitting results
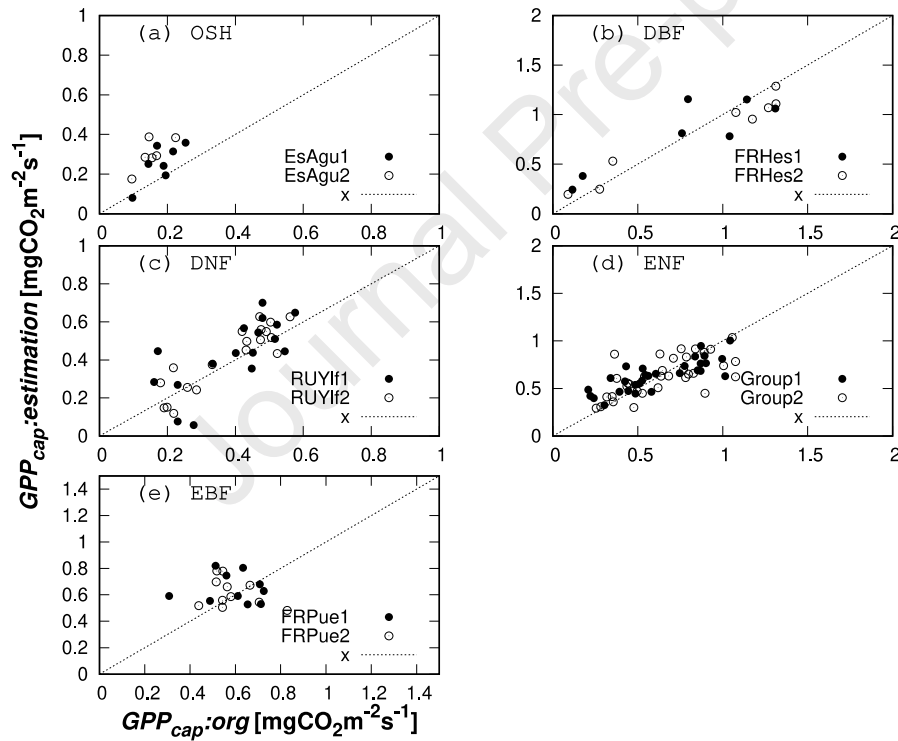
362 and their one sigma values; asterisks (*) indicate data newly added in this study.

363

364 Table 4. Relationship between GP2000 and CI_{green} for each vegetation type.

Vegetation types (IGBP class) (IGBP class)	$GP2000$ min.	max.	ave.	No. of data	$GP2000 = aCI_{green} + b$ a	b	RMSE	R^2	p
Open shrubland (OSH) Savanna (SVA) Grasslands (GRA) Croplands (CRO)	0.01	1.57	0.36	123	0.4±0.01	-0.28 ±0.02	0.11	0.94	<0.001
Deciduous broadleaf forest (DBF) Closed shrubland (CSH)	0.02	1.32	0.58	49	0.17±0	-0.34±0.07	0.19	0.81	<0.001
Deciduous needleleaf forest (DNF)	0.16	1.66	0.52	45	0.24±0.01	-0.31±0.05	0.14	0.87	<0.001
Red pine of JP-FJY (ENF)	0.51	1.26	0.96	9	0.18±0.04	0.15±0.18	0.11	0.76	0.002
Evergreen needleleaf forest (ENF)	0.21	1.08	0.63	65	0.15±0.02	0.03±0.07	0.17	0.54	<0.001
Evergreen broadleaf forest (EBF)	0.32	1.37	0.73	27	0.16±0.03	-0.09±0.17	0.18	0.51	<0.001

365

366

Figure 7. Cross-validation of linearity in each vegetation group for newly added data. (a) ES-Agu data for open shrubland (OSH), savanna (SAV), and grassland (GRA). (b) FR-Hes1 data for deciduous broadleaf forest (DBF) and closed shrubland (CSH). (c) RU-YLF data for deciduous needleleaf forest (DNF). (d) Half of the NL-Loo, IT-Lav and RU-YPF data, and (e) FR-Pue data for EBF.

372

373 The results of the cross-validation are shown in Fig. 7. For ES-Agu, the GPP

374 capacity estimated from the linear relationship in Equation (3) was higher than the

375 Flux GPP. For the other sites, estimates were distributed near the 1:1 line. The root

376 mean square error (RMSE) values for OSH, DBF, DNF, ENF, and EBF were 0.07,

377 0.07, 0.02, 0.005, and 0.07, respectively.

378

379 ***3.3. The GPP/GPP capacity ratio based on flux data***

380 The seasonal variation in the GPP/GPP capacity ratio of evergreen needleleaf

381 forests was stable over the year, and the yearly value of the ratio was higher than

382 0.94 (Fig. 8). For the other vegetation groups, the tendency of seasonal variation

383 in the ratio was dependent on the site. For evergreen broadleaf forest, the seasonal

384 variation at TH-SKR was stable over the year, with a maximum value of 0.961,

385 but at FR-Pue, it was lower and decreased from July to September. In deciduous

386 needleleaf forests, the seasonal variation in the ratio at RU-YLF was stable over

387 the year, with an annual value of 0.953, whereas at JP-TMK, it was not stable over

388 time and the annual value (0.680) was lower than that at RU-YLF. For deciduous

389 broadleaf forest and wetland, there was slight seasonal variation. The ratio

390 decreased slightly from June in the growing season. For the rice paddy site at JP-

391 MSE, the ratio was stable, with an annual value of 0.917. The annual value for

392 open shrubland was lower than those of all forest types, except at JP-TMK. There

393 was considerable noise in the ratio, which was higher than in the ratio for open

394 shrubland when GPP was lower than 1 $gCO_2m^{-2}day^{-1}$. The use of this method was

395 considered to be limited when GPP was low. For sites with a stable ratio close to

396   one, the GPP capacity was considered a first-order approximation of GPP.

397
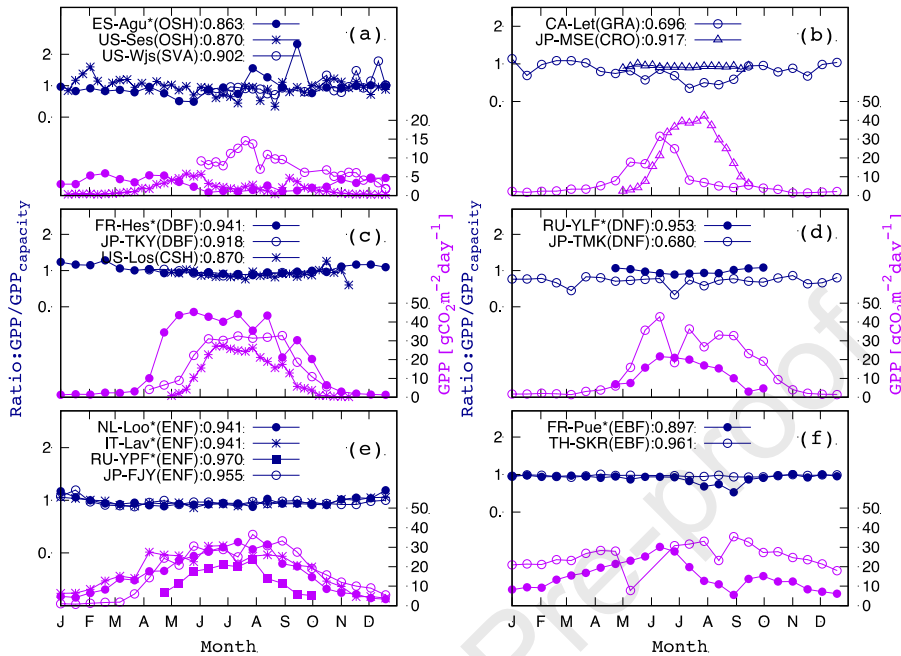
398

Figure 8. Seasonal variation of flux data in the daily GPP/GPP capacity ratio (blue) and GPP (pink)

for (a) open shrubland (OSH) and savanna (SAV), (b) cropland (CRO) rice paddy and grassland

(GRA), (c) deciduous broadleaf forest (DBF) and closed shrubland (CSH) in a permanent wetland,

(d) deciduous needleleaf forest (DNF), (e) evergreen needleleaf forest (ENF), and (f) evergreen
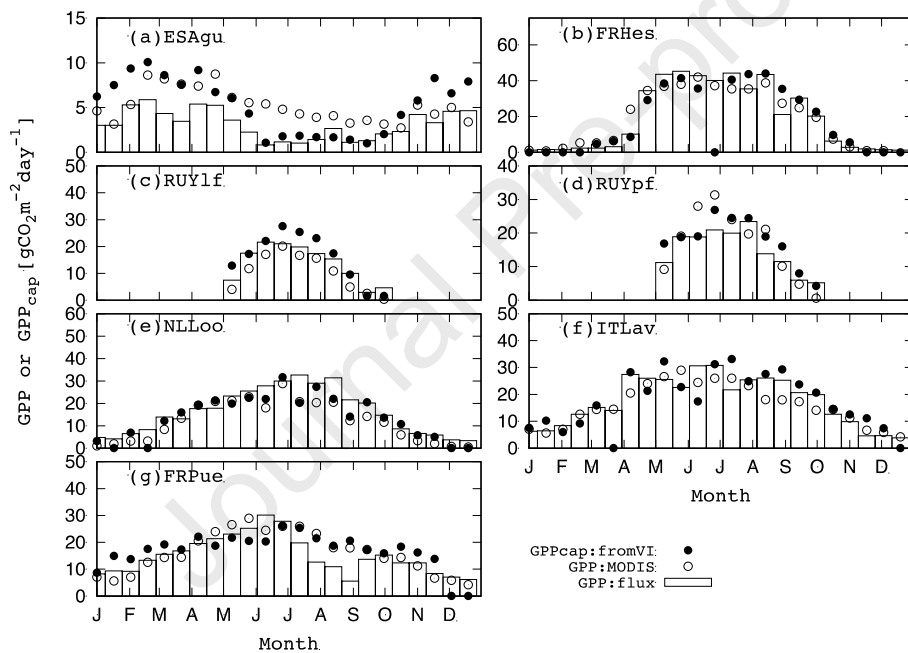
broadleaf forest (EBF).

404

3.4. Daily and diurnal variation in GPP capacity from MODIS CI_{green} for the newly

added flux sites

407   Next, we applied our algorithm to satellite data to estimate GPP capacity. The

408   daily GPP capacity from MODIS CI_{green} at the newly added flux locations was

409   compared to the daily Flux GPP and MODIS GPP products (Fig. 9). The capacity

410   estimated from the CI_{green} at ES-Agu was overestimated in winter but reproduced

411   the depression in summer Flux GPP well. The MODIS GPP product reproduced

412   some of the winter Flux GPP well but not the summer Flux GPP depression. Both

413   the FR-Hes estimates and MODIS GPP product captured the seasonal changes in

414   Flux GPP. The RU-Ylf estimates were higher than the MODIS GPP product, and

415   both approximately captured the seasonal patterns of Flux GPP. Both the RU-Ypf

416   estimates and MODIS GPP product were reproduced well in some months but not

417   in others. The NL-Loo estimate and MODIS GPP product were nearly identical

418   but were lower than the Flux GPP from July to September. The IT-Lav and FR-

419   Pue estimates and the MODIS GPP product were reproduced well in some months

420   but not in others.

421

422   Figure 9. Daily GPP capacity from the CI_{green}, daily GPP of flux data, and MODIS GPP product

423   for (a) ES-Agu (open shrubland [OSH]), (b) FR-Hes (deciduous broadleaf forest [DBF]), (c) RU-

424   YLF (deciduous needleleaf forest [DNF]), average value for 2004−2007, (d) RU-Ypf (evergreen

425   needleleaf forest [ENF]), average value for 2004−2007, (e) NL-Loo (ENF), (f) IT-Lav (ENF),

426   and (g) FR-Pue (evergreen broadleaf forest [EBF]). CI_{green} was not available in late June for FR-

427   Hes and late May for ITLav.

428

429   One of the key features of the algorithm used in this study was its ability to

430 calculate diurnal changes in the instantaneous GPP capacity using an LRC. Fig.

431 10 shows examples of the diurnal variation in the instantaneous GPP capacity. An

432 example of the overestimation of the diurnal variation in the instantaneous GPP

433 capacity from MODIS CI_{green} was the ES-Agu site on Mar. 6 (Fig. 10 (a1)), which

434 corresponded to a period when the daily GPP capacity was also overestimated in

435 Fig. 9 (a). Conversely, another example at ES-Agu on May 9 (Fig. 10 (a2)),

436 showed that the GPP capacity was slightly higher than the Flux GPP capacity, but

437 was estimated well. The GPP capacity of Flux and from MODIS CI_{green} were

438 nearly identical during the early morning and late afternoon. The midday

439 depression of photosynthesis, which is the drop from the GPP capacity, was

440 observed around noon in GPP. The GPP capacities from MODIS CI_{green} were

441 slightly higher or lower than the Flux GPP capacity. Midday depressions in Flux

442 GPP were also observed at NL-Loo in April and FR-Pue in July.
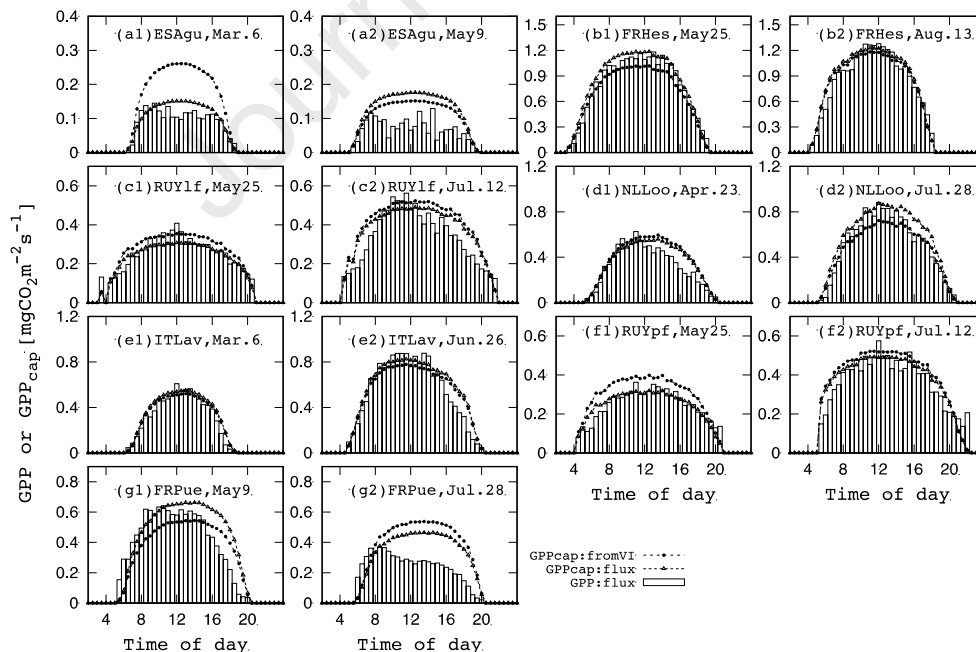
443

444 Figure 10. Diurnal variation in the instantaneous GPP capacity from MODIS CI_{green} and from

445 Flux data, and in Flux GPP for (a1, 2) ES-Agu (open shrubland [OSH]), (b1, 2) FR-Hes

446   (deciduous broadleaf forest [DBF]), (c1−2) RU-Ylf (deciduous needleleaf forest [DNF]), (d1, 2)

447   RU-Ypf (evergreen needleleaf forest [ENF]), (e1, e2) NL-Loo (ENF), (f1−f2) IT-Lav (ENF), and

448   (g1, 2) FR-Pue (evergreen broadleaf forest [EBF]).

449

450   **4. Discussion**

451   *4.1. Initial slope of the LRC parameters derived from flux data*

452   At the leaf level, the initial slope of the LRC is the apparent quantum efficiency, which

453   is related to the total leaf chlorophyll content. The initial slope αP_{max} for the GPP capacity

454   in Equation (2) showed the seasonal variation (Fig. 5) at the canopy level; P_{max} caused

455   the seasonal variation. GP2000 convertible to P_{max} had a linear relationship with CI_{green},

456   which is correlated with chlorophyll content, as seasonal changes in αP_{max} for GPP

457   capacity are considered to be related to seasonal changes in canopy chlorophyll content.

458   Previous studies of the net ecosystem exchange (NEE) that did not focus on unstress

459   conditions reported the similar results, *i.e.*, the initial slope (Q in Equation (5)) of the LRC

460   showed seasonal variation and was similar to that of P_{max} in a temperate mixed forest

461   (Zhang, *et al.*, 2006); sagebrush steppe, short grass steppe, and mixed grass prairie (Polly

462   *et al.*, 2009); and semi-arid grassland (You *et al.*, 2022). Q and P_{max} have a linear

463   relationship in various biome types, including ENF, EBF, MF (mixed Forest), GRS, SVN,

464   and TND (tundra) (Saito *et al*., 2009). The initial slope Q in Equation (5) equals αP_{max} in

465   Equation (5), as seasonal changes in P_{max} cause similar seasonal patterns and there is a

466   linear relationship between the two parameters.

467

468   The units of α and α_{ave} is the inverse of the incident photosynthetic photon flux density

469   (PPFD), and it was hypothesized that $1/\alpha_{ave}$ represents the light environment. In evergreen

470   broadleaf forest, $1/\alpha_{ave}$ values were higher at TH-SKR than at FR-Pue, with the latitude

471   of TH-SKR being lower than that of FR-Pue. Regarding the evergreen needle leaf and

472   deciduous needle leaf types, the high-latitude sites RU-YPF and RU-YLF had the lowest

473    $1/\alpha_{ave}$ values for the same plant types. Lin *et al.* (2024) showed that the initial slope (α_{ave}

474   P_{max} in this study) tended to decrease with increasing latitude, with P_{max} varying weakly

475   with latitude for 64 typical ecosystems of ChinaFLUX ecosystem measurements over 20

476   years. Our results showed a similar decrease in α_{ave} (increasing as $1/\alpha_{ave}$) with increasing

477   latitude. However, not all of the differences in $1/\alpha_{ave}$ values could be explained based only

478   on the latitude of the sites. For example, at site NL-Loo, the latitude was slightly higher,

479   but the value of $1/\alpha_{ave}$ was not as low as those expected ranges. This was likely due to the

480   fact that plants in NL-Loo gather light for optimal photosynthesis than plants at the same

481   latitude. Additionally, the topography around this location is less undulating. One

482   possible reason for these differences is that Equation (2) used the incident PPFD (not

483   absorbed PPFD) because $1/\alpha_{ave}$ values would be affected by leaf angles. The leaf angle

484   could be a critical parameter for plants to achieve optimal photosynthesis performance

485   (Yang, *et al.*, 2023). For example, if the leaf angle is perpendicular to sunlight, more light

486   is available. On the other hand, if the leaf angle is steeper, more light is not available, but

487   irradiation light can be reduced to maximize carbon gain (Falster *et al.*, 2003).

488   Furthermore, plants adjust leaf angles over the short or long term in response to

489   environmental and biological drivers (Yang, *et al.*, 2023). Thus $1/\alpha_{ave}$ may differ from the

490   values expected based on latitude because leaf angles can be adjusted to collect

491   appropriate light within the canopy. Further studies using other flux sites are needed to

492   confirm this hypothesis.

493

494 ***4.2. Relationship between CI_green and GP2000***

495 The liner relationship between GP2000 and CI_{green} for the newly added data was similar

496 for the same vegetation type, even though the continents were different. The relationship

497 between them showed hysteresis, particularly in deciduous broadleaf forests, as shown in

498 Fig. 6. The reason for focusing on the linear relationship between the two parameters is

499 that there may have been pixels that were not occupied by uniform vegetation cover. A

500 nonlinear relationship increases the uncertainty of estimations in heterogeneous pixels.

501

502 The Farquhar photosynthesis model parameters of the potential electron transport rate

503 (J_{max}) and maximum carboxylation rate (V_{Cmax}) have strong linear correlations with leaf

504 chlorophyll content in leaves (Wullschleger, 1993). This is because plants optimize their

505 resource allocation to preserve the balance between their enzymatic Rubisco and

506 chlorophyll capabilities (Wullschleger, 1993). Within deciduous forests, V_{Cmax} values

507 have a stronger linear relationship with the chlorophyll content of a canopy than with J_{max}

508 values (Croft *et al.*, 2017). Typically, the J_{max} values are approximately double the V_{Cmax}

509 values (Leuning, 1997; Hikosaka *et al.*, 2007), and seasonal changes in V_{Cmax} values have

510 been shown to regulate P_{max} when the intercellular partial pressure of CO_2 is

511 approximately 20 Pa in canopy leaves (this study was on *Q. crispula* in a cool temperate

512 forest; Hikosaka *et al.*, 2007). Therefore, we believed that GP2000, which is the

513 parameter responsible for high PAR under low-stress conditions, would be limited by

514 V_{Cmax}. There was a strong correlation between V_{Cmax} and chlorophyll content. This was

515 also true for CI_{green} because there was a linear relationship between GP2000 and CI_{green}.

516

517 Furthermore, previous studies of NEE including both stressed and non-stressed

518 conditions reported that the interannual variability in P_{max} is positively correlated with

519 LAI (Laurila *et al.*, 2001; Polly *et al.*, 2009; Gilmanov, *et al.*, 2010; Zhang *et al.*, 2012;

520 Tong *et al.*, 2014; You *et al.*, 2022). From the perspective of photosynthesis processes,

521 changes in LAI imply changes in canopy chlorophyll content. Given the seasonal changes

522 in the canopy chlorophyll content, our assumption that the LRC parameter P_{max} is related

523 to the canopy chlorophyll content under low-stress conditions was considered reasonable.

524

525 Hysteresis has been reported in the relationships between the daily P_{max} and vegetation

526 indices based on red-edge wavelength, such as the NDVI, EVI, and CI (Muraoka *et al.*,

527 2013; Gitelson *et al.*, 1994), with the NDVI formula $= (R_{750} - R_{705})/(R_{750} + R_{705})$ in a

528 deciduous broadleaf forest (JP-TKY) (Sims *et al.*, 2002). A curvilinear hysteresis was

529 observed, particularly from spring to midsummer. By contrast, the canopy chlorophyll

530 index (CCI), which is based on the ratio of the derivative of the red-edge wavelength

531 range (CCI $= D_{715-725}/D_{695-705}$) (Sims *et al.*, 2006), has an almost linear relationship with

532 the daily P_{max} from spring to midsummer and from midsummer to early winter (Muraoka

533 *et al.*, 2013). The seasonal patterns of leaf reflectance of *B. ermanii* and *Q. crispula* at the

534 JP-TKY site indicated a low chlorophyll content, possibly due to carotenoid effects.

535 Young leaves had a higher green reflectance and lower NIR reflectance than mature

536 leaves, with the NIR reflectance reflecting the developmental pattern of the mesophyll

537 structure (Noda *et al.*). Young thin leaves have a lower NIR reflectance because the

538 mesophyll structure is too underdeveloped. The NIR reflectance of CI_{green} was used as a

539 baseline because it is not sensitive to chlorophyll content. The lower NIR reflectance in

540 young leaves would result in lower CI_{green} values than expected due to the actual

541 chlorophyll content. This lower NIR reflectance in the leaf development period may have

542   caused one-way hysteresis. In a mixed temperate forest, the midday GPP and total

543   chlorophyll content in the canopy (Chl_{canopy}) multiplied by the PAR have a linear

544   relationship mid-season; however, the slope of the relationship was slightly lower in mid-

545   season than at the start or end of the season (Croft *et al.*, 2015). The characteristics of leaf

546   gas exchange vary in the leaf expansion period and in mature leaves (Kosugi *et al.*, 2006).

547   From the seasonal patterns of the chlorophyll content, the light-saturated photosynthetic

548   rate (i.e., P_{max}), maximum carboxylation rate at 20°C (V_{Cmax20}), and potential electron

549   transport rate at 20°C (J_{max20}) for *B. ermanii* and *Q. crispula* in JP-TKY have been

550   determined (Noda *et al.*, 2015). The P_{max} and V_{Cmax20} decreased approximately 10 days

551   earlier than the chlorophyll content and J_{max20} decreased during the senescence period.

552   Considering these previously reported findings, the lower photosynthetic capacity in the

553   leaf senescence period than in the mature leaf period, with the same amount of chlorophyll

554   in both periods, likely caused a one-way hysteresis in the leaf senescence period.

555

556   A seasonal change was clearly detected among deciduous plant functional types (PFTs),

557   and the relationship between CI_{green} and GP2000 was determined. By contrast, evergreen

558   PFTs have green leaves throughout the year, and the ranges of CI_{green} and GP2000 were

559   not large, except at JP-FJY, where a change in leaf color was observed. For the small

560   ranges of CI_{green} and GP2000 throughout the year, it was impossible to determine their

561   relationship based on data from only one site. In this study, the CI_{green} and GP2000

562   distributions of ENF at annual air temperatures of −10°C to 10°C showed a broad linear

563   relationship (Fig. 6 (e)).

564

565   Theoretically, if CI_{green} represents the chlorophyll content, it should be zero when GP2000

566   is zero. The zero intercept of the relationship between CI_{green} and GP2000 represents this

567   point in the relationship. A near zero value of the intercept was observed for evergreen

568   vegetation types and a negative value was observed for herbaceous and deciduous

569   vegetation types (Fig. 6). Herbaceous and deciduous vegetation areas have seasons with

570   no green vegetation, resulting in similar spectral reflectances of withered leaves and

571   sometimes soil. CI_{green} was almost 1 when the GP2000 is zero, which means that the

572   R_{NIR}/R_{green} ratio was close to 2. The spectral reflectance of withered leaves and soil at

573   green wavelengths was higher than that of green vegetation, with a R_{NIR}/R_{green} ratio close

574   to 2.

575

576   Herbaceous vegetation dominated sites with higher slopes. Herbaceous and woody plants

577   have a different canopy structure and light enters the canopy differently. Peng *et al.*

578   (2017) analyzed the relationship between the canopy chlorophyll content and a vegetation

579   index for maize and soybean using hyperspectral radiometer data and found that the

580   relationship was the same between crops with different canopy structures under a $CI_{red\text{-}}$

581    $_{edge}$. Their study of herbaceous crops is one example of the response of a vegetation index

582   to vegetation under different canopy structures. The $CI_{red\text{-}edg}$ determined with the Sentinel-

583   2/MSI sensor is the most promising candidate for the development of a sensitive index of

584   canopy chlorophyll under different canopy structures. In addition, the relationship

585   between GP2000 and the chlorophyll content of the canopy itself must be studied.

586

587   ***4.3. Estimation of GPP capacity from satellite data and the applicable scope of the***

588   ***model***

589   The proposed approach used LRC to estimate instantaneous GPP capacity and was

590   able to estimate instantaneous GPP capacity on a sub-day scale. The diurnal

591   variation in the instantaneous GPP observed under high stress indicates that the

592   photosynthesis rate increases as increasing light intensity when weather conditions

593   are appropriate for photosynthesis in the morning, then high-stress conditions

594   cause stomata closure and decrease the photosynthesis rate, and after the stress

595   alleviated, the stomata reopen and photosynthesis rates increase again. These

596   phenomena were observed not only at the leaf level (Kamakura *et al.*, 2011, 2012,

597   2021) but also at the canopy level (Fig. 10 (a1, 2; d1)). The instantaneous GPP

598   capacity on a sub-day scale was calculated from LRC (Fig. 10). The parameter

599   P_{max} was estimated from CI_{green}, and α_{ave} was determined for each vegetation type

600   from the flux data. The instantaneous Flux GPP showed a drop from the

601   instantaneous GPP capacity (Fig. 10 (a1, 2; c2; d1; g1, 2)). From this result, the

602   instantaneous GPP capacity could be considered the baseline of the instantaneous

603   GPP under unstressed condition. Furthermore, the midday depression will be able

604   to be calculated from the area between the baseline and GPP. Thus the baseline of

605   instantaneous GPP at the sub-day scale is important for quantifying midday

606   depression.

607

608   The proposed approach used GPP selected under low-stress conditions using

609   atmospheric dryness (VPD) to determine the LRC parameters, although low soil

610   water content (SWC) can affect GPP. There is often a correlation between VPD

611   and SWC, making it difficult to distinguish effects on GPP reduction and canopy-

612   level stomatal conductance. Recently, Liu *et al.* (2020) reported that soil moisture

613   (SM) dominates dryness stress rather than VPD when studying solar-induced

614 fluorescence as an indicator of GPP with SM and VPD. By contrast, Kimm *et al.*,

615 (2020) reported the results of a path analysis to characterize connections among

616 environmental variation in precipitation, SWC, relative humidity (RH), air

617 temperature (Ta), VPD, and canopy-level stomatal conductance (Gs). SWC affects

618 both RH and Ta, which both determine VPD, which makes a dominant

619 contribution to Gs at hourly and daily scales at AmeriFlux sites, where soybean

620 and corn grow in U.S. Corn Belt. Furthermore, Fu *et al.* (2022) reported that both

621 GPP and Gs had negative sensitivity to increasing VPD across the entire range of

622 SWC at 15 sites major ecosystems sites across Europe over a 5-year period that

623 included extreme summer drought, and showed negative sensitivity to decreasing

624 SWC mainly at a restricted range of low SWC values. Based on these findings, we

625 considered it reasonable to select less water stress data based on VPD at the diurnal

626 scale, as canopy-level stomatal closure responds to increased VPD and VPD

627 reflects decreased SWC.

628

629 Vegetation at high latitudes grows under low temperatures. The example of May

630 at the RU-YLF site included a low air temperature in the early morning, as shown

631 in Fig. D1. Early morning leaf and air temperatures were cooler and solar radiation

632 intensity was lower, possibly preventing stomatal opening. This issue must be

633 addressed in future studies.

634

635 Lin *et al.* (2024) reported significant spatial heterogeneity in average LRC

636 parameters during the growing season, varying with plant species and vegetation

637 cover due to geographic variation in environmental factors. CI_{green}, derived from

638   satellite sensor data, was closely linked to canopy chlorophyll content and

639   reflected vegetation cover and density across different regions, indicating its

640   potential to capture plant responses to environmental conditions. In our study, the

641   relationship between CI_{green} and GP2000, which is important for determining the

642   LRC parameter P_{max}, was applicable to the same vegetation groups, even of

643   different continents, which is likely advantageous for obtaining LRC parameters

644   in various geographic regions globally. When estimating the GPP capacity using

645   this relationship, the estimation error would be larger than that determined at size-

646   restricted sites, as shown in Fig. 7. For a particular region, it would be better to

647   use relationships specific to that region to reduce the estimation error.

648

649   Plant responses to climate change are complex due to diurnal weather variation,

650   in addition to regional annual mean variation. The decrease in instantaneous GPP

651   diurnal variation can be considered a plant response to diurnal weather variation.

652   Instantaneous GPP capacity can be considered a baseline that is independent of

653   diurnal drought. It remains unclear whether changes in GPP under climate change

654   depend on those in the baseline or the diurnal decrease in photosynthesis. The

655   proposed approach could be used to examine changes in the GPP baseline using

656   satellite observations; furthermore, it can also be applied under severe stress

657   conditions at sub-daily time scales. For such future applications, the midday

658   depression and instantaneous GPP would be derived using the proposed GPP

659   capacity combined with independent stress factor data. For example, canopy-level

660   stomatal regulation would be measurable using high-frequency thermal sensing

661   data obtained by meteorological satellites, with recently improved spatial

662 resolution.

663

5. Conclusions

665 This study investigated the LRC parameters and the relationship between GP2000

666 and CI_{green} across 16 sites spanning tropical to subarctic climates on the Eurasian and

667 North American continents. The average initial slope of the LRC during the growing

668 season was 0.0003–0.0021 $mgCO_2$ (μmol photon)$^{-1}$. A linear relationship between

669 GP2000 ($mgCO_2$ m^{-2} s^{-1}) related to P_{max} and CI_{green}, which is sensitive to canopy

670 chlorophyll content, was observed in most vegetation types, except for deciduous

671 broadleaf forests, where hysteresis occurred. The relationship was strongest in

672 herbaceous-dominated sites, such as open shrubland, savanna, and cropland, with the

673 slope highest at 0.40. Woody plant sites exhibited lower slopes, with the next highest

674 value of 0.24 found in deciduous needleleaf forests, and values ranging from 0.15 to 0.18

675 for other vegetation types (deciduous broadleaf forest, evergreen needleleaf forest,

676 evergreen broadleaf forest). The intercept tended to be negative for deciduous vegetation

677 and close to zero for evergreen types.

678

679 The yearly GPP/GPP capacity ratio was close to one at the canopy level. When applied

680 to satellite data, the method produced seasonal patterns in daily GPP capacity that were

681 similar with MODIS GPP products and Flux GPP. The diurnal variation in instantaneous

682 GPP capacity showed that under high dryness, Flux GPP decreased around noon but was

683 nearly identical to GPP capacity in the early morning and late afternoon. Instantaneous

684 GPP capacity can be considered a baseline for stress-free conditions, crucial for

685 quantifying midday depression at sub-day scales.

686

687   Further research should focus on developing more sensitive indices, such as those based

688   on the red-edge band or total canopy chlorophyll content. The proposed method has

689   potential applications under severely stressed conditions and at sub-daily time scales.

690   High-frequency thermal sensing data from meteorological satellites with improved spatial

691   resolution could be used to measure canopy-level stomatal regulation, enhancing our

692   understanding of instantaneous GPP under varying environmental stresses.

693

694   **CRediT authorship contribution statement**

695   Conceptualization: KM, NS; Methodology: KM, EY; Formal Analysis: KM, EY;

696   Investigation: KM, EY; Resources; KM, NS, ALB; Data Curation: KM, EY, ALB, JT;

697   Writing - original draft: KM; Writing - review and edit- ing: KM, NS, ALB, JT; Project

698   administration: KM; Funding Acquisition: KM, NS, ALB.

699

700   **Declaration of Competing Interest**

701   The authors declare that they have no known competing financial interests or personal

702   relationships that could have appeared to influence the work reported in this paper.

703

727

728   **Appendix A.**

729   Based on the flux data from Siberia, GPP was calculated using net ecosystem production

730   (NEP) plus ecosystem respiration (Rec), as follows:

731    $$GPP(T_{air}) = NEP + Rec(T_{air}) \qquad (A.1)$$

732   where Rec is plant respiration plus soil respiration as a function of air temperature (T_{air}).

733   The nighttime Rec was calculated as an exponential function of T_{air} to fit nighttime NEP

734   as a function of T_{air} as follows:

735   $$Rec(T_{air}) = aexp(bT_{air}) \quad\quad\quad\quad (A.2)$$

736

737   where a and b are empirical constants determined through regression, with b related to

738   the temperature coefficient and the Rec considered at 0°C. Nighttime data were selected

739   when the friction velocity was higher than 0.2 ms^{-1} and the relative humidity was less

740   than 100% for data with NEP > 0. The parameters a and b for the YLF site were 0.068 ±

741   0.002 and 0.029 ± 0.02, respectively, and those for the YLP site were 0.065 ± 0.002 and

742   0.039 ± 0.003, respectively.

743

744   **Appendix B**
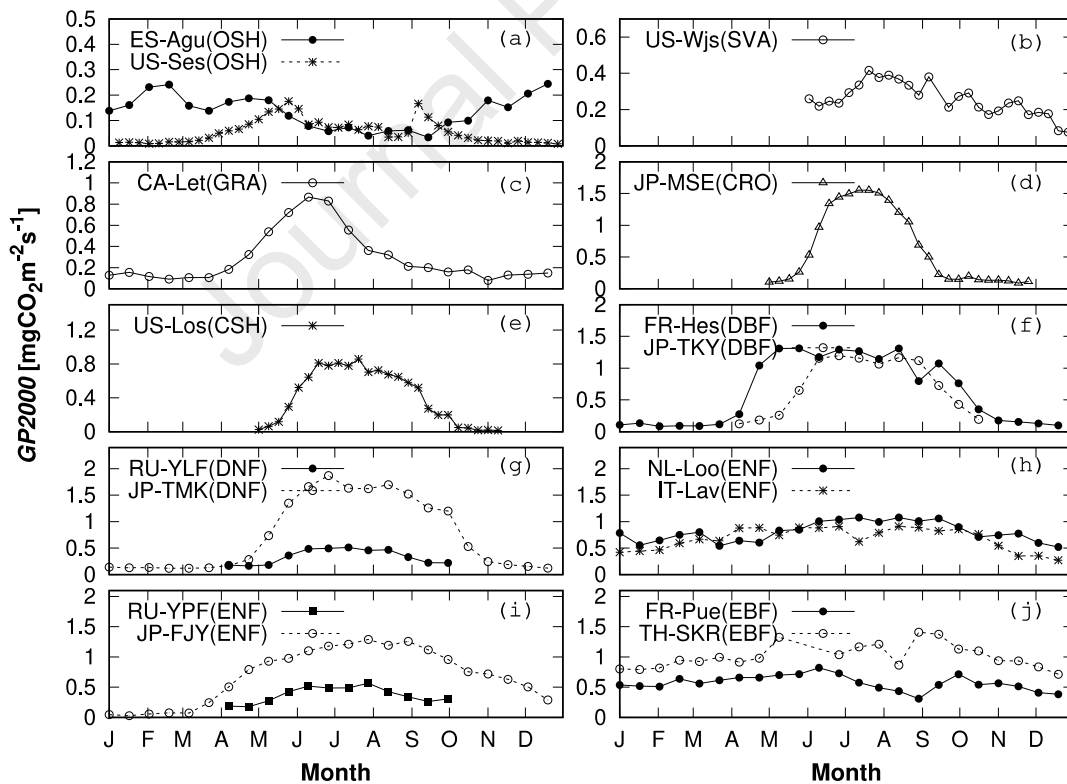
745

746   Figure B1. Seasonal changes in GP2000 for (a) open shrubland (OSH), (b) savanna (SVA), (c) grassland

747   (GRA), (d) cropland (CRO) rice paddy, (e) closed shrubland (CSH) of permanent wetland, (f) deciduous

748   broadleaf forest (DBF), (g) deciduous needleleaf forest (DNF), (h, i) evergreen needleleaf forest (ENF),

749   and (j) evergreen broadleaf forest (EBF).

750

751   **Appendix C**
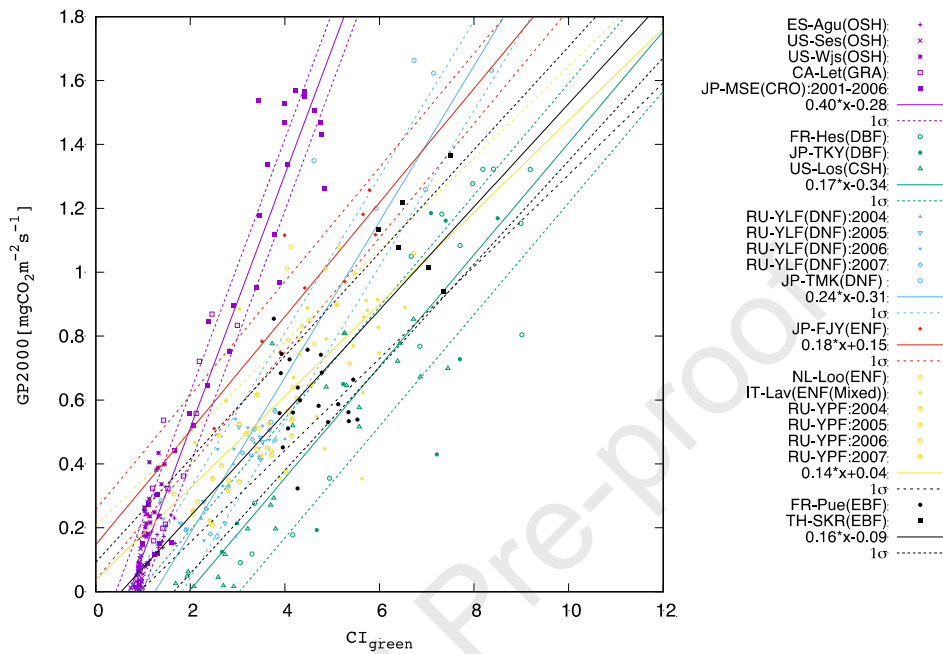
752

753   Figure C1. Relationship between CI_{green} and GP2000 for open shrubland (OSH), savanna (SAV),

754   grassland (GRA), and cropland (CRO) rice paddy (JP-MSE), deciduous broadleaf forest (DBF) and

755   closed shrubland (CSH) in a permanent wetland, deciduous needleleaf forest (DNF), evergreen needleleaf

756   forest (ENF) of *Pinus densiflora* in JP-FJY, and evergreen broadleaf forest (EBF). The solid line

757   represents the fitting results from a linear regression, and the dotted lines indicate the one sigma values

758   for the fitting.

759

760   Appendix D

761
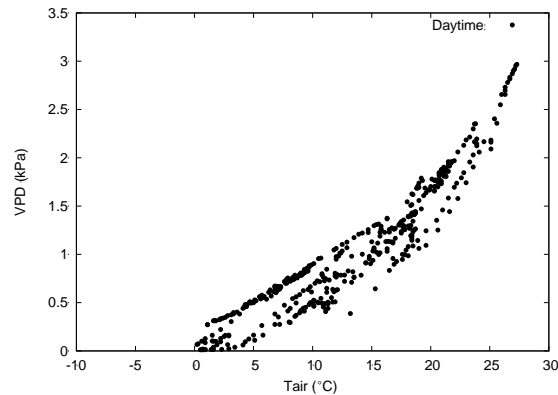
Figure D1. Air temperature and VPD for 16 days from DOY 145 to 161 at the YLF site.

763

764 **References**

765 Aguilos, M.M., Gamo, M., & Maeda, T. (2007). Carbon budget of some tropical and

766 temperate forest. *Asia-Flux Newsletter 2007*, *Special Issue*, 18–22.

767 Anderson-Teixeira, K. J., Delong, J. P., Fox, A. M., Brese, D. A., & Litvak, M. E.

768 (2011). Differential responses of production and respiration to temperature and

769 moisture drive the carbon balance across a climatic gradient in New Mexico. *Global*

770 *Change Biology*, *17–1*, 410–424, DOI: 10.1111/j.13652486.2010.02269.x.

771 Asner, G. P., Wessman, C. A., & Archer, S. (1998). Scale dependence of absorption of

772 photosynthetically active radiation in terrestrial ecosystems. *Ecological*

773 *Applications*, *8(4)*, 1003–1021.

774 Beer, C., Reichstein, M., Tomelleri, E., Ciais, P., Jung, M., Carvalhais, N., Rödenbeck,

775 C., Arain, M. A., Baldocchi, D., Bonan, G. B., Bondeau, A., Cescatti, A., Lasslop,

776 G., Lindroth, A., Lomas, M., Luyssaert, S., Margolis, H., Oleson, K. W., Roupsard,

777 O., Veenendaal, E., Viovy, N., Williams, N., Woodward, F. I., & Papale, D. (2010).

778 Terrestrial gross carbon dioxide uptake: global distribution and covariation with

779 climate. *Science, 329(5993)*, 834–838.

780   Croft, H., Chen, J.M., Froelich, N.J., Chen, B., & Staebler, R.M. (2015). Seasonal

781   controls of canopy chlorophyll content on forest carbon uptake: Implications for

782   GPP modeling. *Journal of Geophysical Research: Biogeosciences*, *10.1002*, 1576–

783   1586.

784   Croft, H., Chen. J.M., Luo, X., Bartlett, P, Chen, B., & Staebler, R. (2017). Leaf

785   chlorophyll content as a proxy for leaf photosynthetic capacity. *Global Change*

786   *Biology*, *23*, 3513–3524.

787   Dash, J., & Curran, P. J. (2004). The MERIS terrestrial chlorophyll index. *International*

788   *Journal of Remote Sensing*, *25(23)*, 5403–5413.

789   Dash, J., & Curran, P. J. (2007). Evaluation of the MERIS terrestrial chlorophyll index

790   (MTCI). *Advances in Space Research*, *39*, 100–104.

791   Dash, J., Curran, P. J., Tallis, M. J., Llewellyn, G. M., Taylor, G., & Snoeij, P. (2010).

792   Validating the MERIS Terrestrial Chlorophyll index (MTCI) with ground

793   chlorophyll content data at MERIS spatial resolution. *International Journal of*

794   *Remote Sensing*, *31(20)*, 5513–5532.

795   Dolman, A. J., Moors, E. J., & Elbers, J. A. (2002). The carbon uptake of a mid-latitude

796   pine forest growing on sandy soil. *Agricultural and Forest Meteorology*, *111*, 157–

797   170.

798   Falster, D. S., & Westoby, M. (2003). Leaf size and angle vary widely across species:

799   What consequences for light interception? *New Phytologist*, *158*, 509–525.

800   Farquhar, G.D., von Caemmerer, S., & Berry, J.A. (1980). A biochemical model of

801   photosynthetic CO_2 assimilation in leaves of C3 species. *Planta*, *149*, 78–90.

802   Flanagan, L.B., & Adkinson, A.C. (2011). Interacting controls on productivity in a

803   northern Great Plains grassland and implications for response to ENSO events.

804   *Global Change Biology*, *17*, 3293–3311.

805   Fu, Z., Ciais, P., Prentice, C., Gentine, P., Makowski, D., Bastos, A., Luo, X., Green, J.

806   K, Stoy, P. C., Yang, H., & Hajima, T. (2022). Atmospheric dryness reduces

807   photosynthesis along a large range of soil water deficits. *Nature Communications*,

808   *13*, *989.* https://doi.org/10.1038/s41467-022-28652-7.

809   Furumi, S., Xiong, Y., & Fujiwara, N. (2005). Establishment of an algorithm to estimate

810   vegetation photosynthesis by pattern decomposition using multi-spectral data.

811   *Journal of The Remote Sensing Society of Japan*, *25*, 47–59.

812   Gitelson, A. A., & Merzlyak, M. N. (1994). Spectral reflectance changes associated with

813   autumn senescence of *Aesculus hippocastanum* L. and *Acer platanoides* L. leaves.

814   Spectral features and relation to chlorophyll estimation. *Journal of Plant*

815   *Physiology, 143*, 286–292.

816   Gitelson, A. A., Vina, A., Verma, S. B., Rundquist, D. C., Arkebauer, T. J., Keydan, G.,

817   Leavitt, B., Ciganda, V., Burba, G. G., & Suyker, A. E. (2006). Relationship

818   between gross primary production and chlorophyll content in crops: Implications for

819   the synoptic monitoring of vegetation productivity. *Journal of Geophysical*

820   *Research*, *111*, D08S11.

821   Gitelson, A., Viña, A., Solovchenkoe, A., Arkebauerh, T., & Inoue, Y. (2019). Derivation

822   of canopy light absorption coefficient from reflectance spectra. *Remote Sensing of*

823   *Environment*, *213*, 111276, 1–9.

824 Granier, A., Bréda, N., Longdoz, B., Gross, P., & Ngao, J. (2008). Ten years of fluxes
825   and stand growth in a young beech forest at Hesse, North-eastern France. *Annals of*
826   *Forest Science*, *65*, 704.

827 Harazono, Y., Chikamoto, K., Kikkawa, S., Iwata, T., Nishida, N., Ueyama, M., Kitaya,
828   Y., Mano, M., & Miyata, A. (2009). Application of MODIS visible band index,
829   greenery ratio to estimate CO_2 budget of a rice paddy in Japan. *Journal of*
830   *Agriculture and Meteorology*, *65*, 365–374.

831 Harris, A., & Dash, J. (2010). The potential of the MERIS Terrestrial Chlorophyll Index
832   for carbon flux estimation. *Remote Sensing of Environment*, *114*, 1856–1862.

833 Heinsch, F.A., Zhao, M., Running, S.W., Kimball, J.S., Nemani, R.R., Davis, K.J.,
834   Bolstad, P.V., Cook, B.D., Desai, A.R., Ricciuto, D.M., Law, B.E., Oechel, W.C.,
835   Kwon, H., Luo, H., Wofsy, S.C., Dunn, A.L., Munger, J.W., Baldocchi, D.D., Xu,
836   L., Hollinger, D.Y., Richardson, A.D., Stoy, P.C., Siqueira, M.B.S., Monson, R.K.,
837   Burns, S.P., & Flanagan, L.B. (2006). Evaluation of remote sensing based terrestrial
838   productivity from MODIS using regional tower eddy flux network observations.
839   *IEEE Transactions on Geoscience and Remote Sensing*, *44*, 1908–1925.

840 Hikosaka, K, Nabeshima, E., & Hiura T. (2007). Seasonal changes in the temperature
841   response of photosynthesis in canopy leaves of *Quercus crispula* in a cool-
842   temperature forest. *Tree Physiology*, *27*, 1035–1041.

843 Hirata, R., Hirano, T., Saigusa, N., Fujinuma, Y., Inukai, K., Kitamori, Y., & Yamamoto,
844   S. (2007). Seasonal and interannual variations in carbon dioxide exchange of a
845   temperate larch forest. *Agricultural and Forest Meteorology*, *147*, 110–124.

846 Hirata, R., Saigusa, N., Yamamoto, S., Ohtani, Y., Ide, R., Asanuma, J., Gamob, M.,
847   Hirano, T., Kondo, H., Kosugi, Y., Li, S.G., Nakai, Y., Takagi K., Tani, M., & Wang,

848   H. (2008) Spatial distribution of carbon balance in forest ecosystems across East

849   Asia. *Agricultural and Forest Meteorology*, *148*, 761–774.

850 Huete, A.R., Liu, H.Q., Batchily, K., & van Leeuwen., W. (1997) A comparison of

851   vegetation indices over a global set of TM images for EOS-MODIS. *Remote*

852   *Sensing of Environment*, *59(3)*, 440–451.

853 Ide, R., Nakaji, T., & Oguma, H. (2010). Assessment of canopy photosynthetic capacity

854   and estimation of GPP by using spectral vegetation indices and the light-response

855   function in a larch forest. *Agricultural and Forest Meteorology*, *150*, 389–398.

856 Kamakura, M., Kosugi, Y., Tajahashi, S., Matsumoto, K., Okumura, M., & Philip, E.

857   (2011) Patchy stomatal behavior during midday depression of leaf CO_2 exchange in

858   tropical trees, *Tree Physiology*, *31*, 160–168.

859 Kamakura, M., Kosugi, Y., Muramatsu, K., & Muraoka, H. (2012) Simulation and

860   observations of patchy stomatal behavior in leaves of *Quercus crispula*, a cool-

861   temperate deciduous broad-leaved tree species. *J Plant Res*, *125*, 339–349.

862 Kamakura, M., Kosugi, Y., Takanashi, S., Matsuo, N., Uemura, A., & Lion, M. (2021)

863   Temporal fluctuation of patchy stomatal closure in leaves of *Dipterocarpus*

864   *sublamellatus* at upper canopy in Peninsular Malaysia over the last decade,

865   *TROPICS*, *30(3)*, 41–51.

866 Kimm, H., Guan, K., Gentine, P., Wu, J., Bernacchi, C. J., Sulman, B. N., Griffis, T. J.,

867   & Lin, C. (2020). Redefining droughts for the U.S. Corn Belt: The dominant role of

868   atmospheric vapor pressure deficit over soil moisture in regulating stomatal

869   behavior of maize and soybean. *Agricultural and Forest Meteorology*, *287*, 107930,

870   https://doi.org/10.1016/j.agrformet.2020.107930.

871 Kosugi, Y., & Matsuo, N. (2006). Seasonal fluctuations and temperature dependence of

872   leaf gas exchange parameters of co-occurring evergreen and deciduous trees in a

873   temperate broad-leaved forest. *Tree Physiology*, *26*, 1173–1184.

874 Leuning, R. (1997). Scaling to common temperature improves the correlation between

875   the photosynthesis parameters J_{max} and V_{cmax}. *J. of Experimental Botany*, *vol. 48*,

876   *No. 307*, 345–347.

877 Lin, Y., Chen, Z., Yu, G., Yang, M., Hao, T., Zhu, X., Zhang, W., Han, L., Liu, Z., Ma,

878   L., Dou, X., & Luo, W. (2024). Spatial patterns of light response parameters and

879   their regulation on gross primary productivity in China. *Agricultural and Forest*

880   *Meteorology, 345*, 109833. https://doi.org/10.1016/j.agrformet.2023.109833.

881 Liu, L., Gudmundsson, L., Hauser, M. Qin, D., Li, S., & Seneviratne, S. I. Soil moisture

882   dominates dryness stress on ecosystem production globally. (2020). *Nature*

883   *Communications*, *11*, 4892. https://doi.org/10.1038/s41467-020-18631-1.

884 López-Ballesteros, A., Serrano-Ortiz, P., Sánchez-Cañete, Oyonarte, C., & Pérez-Priego,

885   Ó. (2016). Enhancement of the net CO_2 release of a semiarid grassland in SE Spain

886   by rain pulses. *J. Geophys. Res.-Biogeo.*, *121*, 52–66,

887   https://doi.org/10.1002/2015jg003091.

888 López-Ballesteros, A., Kowalski, A.S., Oyonarte, C., Kowalski, A.S., SerranoOrtiz, P.,

889   Sánchez-Cañete, E.P., Moya, M.R., & Domingo, F. (2018). Can land degradation

890   drive differences in the C exchange of two similar semiarid ecosystem?

891   *Biogeosciences*, *15*, 263–278.

892 Laurila, T., Soegaard, H., Lloyd, C. R., Aurela, M., Tuovinen, J.-P., & Nordstroem, C.

893   (2001). Seasonal variations of net CO_2 exchange in European Arctic ecosystems.

894   *Theor. Appl. Climatol.*, *70*, 183–201.

895   Marcolla, B., Pitacco, A., & Cescatti, A. (2003). Canopy architecture and turbulence

896   structure in a coniferous forest. *Boundary-Layer Meteorology*, *108*, 39–59.

897   Matsumoto, K., Ohta, & Tanaka, T. (2005). Dependence of stomatal conductance on

898   leaf chlorophyll concentration and meteorological variables. *Agricultural and Forest*

899   *Meteorology*, *132*, 44–57.

900   Mineshita, Y., Muramatsu, K., Soyama, N., Thanyapraneedkul, J., & Daigo, M. (2016).

901   Determination of parameters for shrubs in the global gross primary production

902   capacity estimation algorithm. *J. of Remote Sensing Society of Japan*, *3*, 236–246.

903   Mizoguchi, Y., Ohtani, Y., Takannashi, S., Iwata, H., Yasuda, Y., & Nakai, U. (2012).

904   Seasonal and interannual variation in net ecosystem production of an evergreen

905   needleleaf forest in Japan. *Journal of Forest Research*, *17(3)*, 283–295.

906   Monteith, J. L. (1972). Solar radiation and production in tropical ecosystem. *Journal of*

907   *Applied Ecology*, *9*, 747–766.

908   Muramatsu, K., Ono, K., Soyama, N., Thanyapraneedkul, J., Miyara, A., & Mano, M.

909   (2017). Determination of rice paddy parameters in the global gross primary

910   production capacity estimation algorithm using 6 years of JP-MSE flux observation

911   data. *Journal of Agricultural Meteorology 7*, *73(3)*, 119–132.

912   Muramatsu, K., Canopy conductance index for GPP estimation from its capacity, *Proc.*

913   *SPIE 10777, Land Surface and Cryosphere Remote Sensing IV*, 107770M (24

914   October 2018); doi: 10.1117/12.2324247.

915   Muraoka, H., Noda, H. M., Nagai, S., Motohka, T., Saitoh, T. M., Nasahara, K. N., &

916   Saigusa, N. (2013). Spectral vegetation indices as the indicator of canopy

917   photosynthetic productivity in a deciduous broadleaf forest. *Journal of Plant*

918   *Ecology*, *6(5)*, 393–407.

919   Myneni, R.B., & Williiams, D. L. (1994). On the relationship between FA-PAR and

920   NDVI. *Remote Sensing and Environment*, *49*, 200–211.

921   Myneni, R.B., Hoffman, S., Knyazikhin Y., Privette, J.L., Glassy J., Tian Y., Wang, Y.,

922   Song X., Zhang Y., Smith G.R., Lotsch A., Friedl M., Morisette J.T., Votava P.,

923   Nemani R.R., & Running, S.W. (2002). Global products of vegetation leaf area and

924   fraction absorbed PAR from year one of MODIS data. *Remote Sensing and*

925   *Environment*, *83*, 214–231.

926   Oak Ridge National Laboratory Distributed Active Archive Center (ORNL DAAC)

927   2008. MODIS Collection 5 Land Product Subsets Web Service. ORNL DAAC, Oak

928   Ridge, Tennessee, USA. Accessed June 10, 2016. Subset obtained for MOD09A1

929   product around sites of NL-Loo, FR-Pue, FR-Hes, IT-Ren, IT-Lav and ES-Agu site,

930   and using MODIS Fixed Sites Subsetting Tool

931   (http://daac.ornl.gov/cgibin/MODIS/GR col5 1/mod viz.html), time period: Jan 1,

932   2000 to Dec 31, 2015.

933   Ohta, T., Maximov, T.C., Dolman, A.J, Nakai, T., Molen, M.K., Kononov, A.V.,

934   Maximov, A.P., Hiyama, T., Iijima, Y., Moors, E.J, Tanaka, H., Toba, T., & Yabuki,

935   H. (2008). Interannual variation of water balance and summer evapotranspiration in

936   an eastern Siberian larch forest over a 7-year period (1998-2006). *Agricultural and*

937   *Forest Meteorology*, *148*, 1941–1953.

938   Ono, K., Maruyama, A., Kuwagata, T., Mano, M., Takimoto, T., Hayashi, K.,

939   Hasegawa, H., & Miyata, A. (2013). Canopy-scale relationships between stomatal

940   conductance and photosynthesis in irrigated rice. *Global Change Biology*, *19*, 2209–

941   2220, DOI: 10.1111/gcb.12188

942 Owen, K. E., Tenhunen, J., Reichestein, M., Wang, Q., Falge, E., Geyer, R., Xiao, X.,

943 Stoy, P., Ammann, C., Arain, A., Aubinet, M., Aurela M., Bernhofer, C., Chojnicki.,

944 B.H, Granier., A., Gruenwald, T., Hadley, J., Heinesch, B., Hollinger, D., Knohl. A.,

945 Kutsch., W., Lohila, A., Meyers., T., Moors, E., Moureaux, C., Pilegaard, K.,

946 Saigusa, N., Verma, S., Vesala, T., & Vogel, C. (2007). Linking flux network

947 measurements to continental scale simulations: ecosystem carbon dioxide exchange

948 capacity under non-water-stressed conditions. *Global Change Biology*, *13*, 734–760,

949 DOI: 10.1111/j.1365-2486.2007.01326.x.

950 Pathre, U., Sinha, A.K., Shirke, P.A., & Sane, P.V. (1998). Factors determining the

951 midday depression of photosynthesis in trees under monsoon climate. *Trees*, 12,

952 472–481.

953 Peng, Y., & Gitelson, A.A. (2012). Remote estimation of gross primary productivity in

954 soybean and maize based on total crop chlorophyll content. *Remote Sensing of*

955 *Environment*, 117, 440–448.

956 Peng, Y., Nguy-Robertson, A., Arkebauer, T., & Gitelson, A.A. (2017). Assessment of

957 canopy chlorophyll content retrieval in maize and soybean: Implications of

958 hysteresis on the development of generic algorithms. *Remote Sensing*, *9*, *226*,

959 doi:10.3390/rs9030226.

960 Pessarakli, M. (Ed.). (2005). *Handbook of Photosynthesis*, *2nd ed.* (pp. 287). CRC Press:

961 Boca Raton, FL, USA.

962 Polly, H. W., Emmerich, W., Bradford J. A., Sims, P. L., Johnson, D. A., Saliendra, N.

963 Z., Svejcar, T., Angell, R., Frank, A. B., Phillips, R. L., Snyder, K., & Morga, J.

964 (2009). Physiological and environmental regulation of interannual variability in CO_2

965   exchange on rangelands in the western United States. *Global Change Biology 16*,

966   990–1002, doi: 10.1111/j.1365-2486.2009.01966.x.

967   Rouse, J. W., Hass, R. H, Schell, J. A., & Deerling, D. W. (1973). Monitoring vegetation

968   systems in the Great Plains with ERTS. *Third ERTS Symposium*, *NASA SP-351*, *I*,

969   309–317.

970   Running, S., Mu, Q., & Zha, M. (2015). MOD17A2H MODIS/Terra Gross Primary

971   Productivity 8-Day L4 Global 500m SIN Grid. NASA LP DAAC.

972   http://doi.org/10.5067/MODIS/MOD17A2H.006

973   Saigusa N., Yamamotoa, S., Murayamaa, S., Kondo H., & Nishimura N. (2002). Gross

974   primary production and net ecosystem exchange of a cool temperate deciduous

975   forest estimated by the eddy covariance method. *Agricultural and Forest*

976   *Meteorology*, *112*, 203–215.

977   Saito, M., Maksyutov, S., Hirata, R., & Richardson, A. D. (2009). An empirical model

978   simulating diurnal and seasonal CO_2 flux for diverse vegetation types and climate

979   conditions. *Biogeosciences*, *6*, 585–599.

980   Sims, D.A., Luo, H., & Gamon J. A. (2002). Relationship between leaf pigment content

981   and spectral reflectance across a wide range of species, leaf structures and

982   development stages. *Remote Sensing of Environment*, *81*, 337–354.

983   Sims, D.A., Luo, H., Hastings, S., Oechel, W. C., Rahman, A. F., & Gamon J. A. (2006).

984   Parallel adjustments in vegetation greenness and ecosystem CO_2 exchange in

985   response to drought in a Southern California chaparral ecosystem. *Remote Sensing*

986   *of Environment*, *103*, 289–303.

987   Soudani, K., Hmimina, G., Dufrene, E., Berveiller, D., Delpierre, N., Ourci-val, J. M.,

988   Rambal, S., & Joffre, R. (2014). Relationships between photochemical reflectance

989   index and light-use efficiency in deciduous and evergreen broadleaf forests. *Remote*

990   *Sensing of Environment*, *144*, 73–84.

991   Steffen, W.L., Walker, B.H., Ingram, J.S., & Koch, Q.W. (1992). Global change and

992   terrestrial ecosystems: The operational plan. *Global Change report*, *No.21* (PP 31).

993   The International Geosphere-Biospere Programme: A Study of Global Change

994   (IGBP) of the International Council of Scientific Unions (ICSU) Stockholm

995   Sulman, B.N., Desai, A.R., Cook, B.D., Saliendra, N., & Mackay, D.S. (2009).

996   Contrasting carbon dioxide fluxes between a drying shrub wetland in northern

997   Wisconsin, USA, and nearby forests. *Biogeosciences*, *6(6)*, 1115–1126.

998   Gilmanov, T. G., Aires, L., Belelli, L., Barcza, Z., Baron, V. S., Beringer, J., Billesbach,

999   D., Bonal, D., Bradford, J., Ceschia, E., Cook, D., Corradi, C., Frank, A., Gianelle,

1000   D., Gimeno, C., Gruenwald, T., Guo, H., Hanan, N., Haszpra, L., Heilman, J.,

1001   Jacobs, A., Johnson, D.A., Kiely, G., Li, S.-G., Magliulo, V., Moors, E., Nagy, Z.,

1002   Nasyrov, M., Owensby, C., Pinter, K., Pio, C., Reichstein, M., Sanz, M.J., Scott, R.,

1003   Soussana, J.-F., Svejcar, T., Tuba, Z., & Zhou, G. (2010). Productivity, respiration,

1004   and light-response parameters of world grassland and agro-ecosystems derived from

1005   flux-tower measurements. *Rangeland Ecology Management*, *63*, 16–39. DOI:

1006   10.2111/REM-D-09-00072.1.

1007   Thanyapraneedkul, J., Muramatsu, K., Daigo, M., Furumi, S., Soyama, N., Nishida, K.,

1008   Nasahara, K. N., Muraoka, H., Noda, H. M., Nagai, S., Maeda, T., Mano, M., &

1009   Mizoguchi, Y. (2012). A vegetation index to estimate terrestrial gross primary

1010   production capacity for the global change observation mission-climate (GCOM-C)

1011   second-generation global imager (SGLI) satellite sensor. *Remote Sensing*, *4(12)*,

1012   3689–3720.

1013   Tong, X., Li, J., Yu, Q., & Lin, Z. (2014). Biophysical controls on light response of net

1014 CO_2 exchange in a winter wheat field in the North China Plain. *PLOS ONE*, 9(2),

1015   e89469. doi:10.1371/journal.pone.0089469.

1016   US-Los site's web page: https://ameriflux.lbl.gov/sites/siteinfo/US-Los, DOI:

1017   10.17190/AMF/1246071.

1018   Vermote, E.F., Nazmi, Z. E. S., & Christopher, O. J. (2002). Atmospheric correction of

1019   MODIS data in the visible to middle infrared: first results. *Remote Sensing of*

1020   *Environment*, *83*, 97–111.

1021   Wullschleger, S.D. (1993). Biochemical limitations to carbon assimilation in C_3 plants –

1022   A retrospective analysis of the *A/C_i* curves from 109 species. *J. of Experimental*

1023   *Botany*, *vol. 44*, *No. 262*, 907–920.

1024   Xiao, X., Hollinger, D., Aber, J., Goltz, M., Davidson, E. A., Zhang Q., & Moore, III B.

1025   (2004a). Satellite-based modeling of gross primary production in an evergreen

1026   needleleaf forest. *Remote Sensing of Environment*, *89*, 519–534.

1027   Xiao, X., Zhang Q., Braswell, B., Urbanski, S., Boles, S., Wofsy, S., Moore III, B., &

1028   Ojima, D. (2004b). Modeling gross primary production of temperate deciduous

1029   broadleaf forest using satellite image and climate data. *Remote Sensing of*

1030   *Environment*, *91*, 256–270.

1031   Yang, X., Li, R., Jablonski, A., Stovall, A., Kim, J., Yi, K., Ma, Y., Beverly, D., Phillips,

1032   R., Novick, K., Xu, X., & Lerdau, M. (2023). Leaf angle as a leaf and canopy trait:

1033   Rejuvenating its role in ecology with new technology. *Ecology Letters*, *26*, 1005–

1034   1020, DOI: 10.1111/ele.14215.

1035   You, C., Wang, Y, Tan, X., Zhang, B., Ren, T., Chen, B., Xu, M., & Chen, S. (2022).

1036   Seasonal and interannual variations of ecosystem photosynthetic characteristics in a

1037   semi-arid grassland of northern China. *J. of Plant Ecology*, *15*, 961–976.

1038   https://doi.org/10.1093/jpe/rtac065.

1039   Zhang, L. M., Yu, G. R., Sun, X. M., Wen, X. F., Ren, C. Y., Fu, Y. L., Li, Q. K., Li, Z.

1040   Q., Liu, Y. F., Guan, D. X., & Yan, J. H. (2006). Seasonal variations of ecosystem

1041   apparent quantum yield and maximum photosynthesis rate (P_{max}) of different forest

1042   ecosystems in China. *Agricultural and Forest Meteorology*, *137*, 176–187.

1043   Zhang Q., Middleton, E. M., Margolis, H. A., Drolet, G. G., Barr, A. A., Black, T. A.,

1044   Xiao, X., Braswell, B., Linder, E., Baret, F., & Moore III, B. (2009). Can a satellite-

1045   derived estimate of the fraction of PAR absorbed by chlorophyll ($FAPAR_{chl}$)

1046   improve predictions of light-use efficiency and ecosystem photosynthesis for a

1047   broad aspen forest? *Remote Sensing of Environment*, *113*, 880–888.

1048   Zhang, P., Chen, S., Zhang, W., Miao, H., Chen, J., Han, X., & Lin, G. (2012).

1049   Biophysical regulations of NEE light response in a steppe. *J. of Plant Ecology*, *5(2)*,

1050   238–248. doi: 10.1093/jpe/rtr017.

1051

List of Figure Captions

1053   Figure 1. Diurnal variation in GPP capacity can be calculated from light response curve

1054   of GPP capacity and diurnal variation in photosynthetically active radiation

1055   (PAR).

1056   Figure 2. Light response curve of gross primary production capacity (GPP capacity).

1057   Figure 3. Mean and standard deviation of the GPP capacity LRC parameters for α_{ave} at

1058   16 sites.

1059   Figure 4. Seasonal changes in P_{max} for (a) open shrubland (OSH), (b) savanna (SVA),

1060   (c) grassland (GRA) (d) cropland (CRO) rice paddy, average value over 4 years,

1061   (e) deciduous broadleaf forest (DBF), (f) closed shrubland (CSH) in a permanent

1062   wetland, (g) deciduous needleleaf forest (DNF), RU-YLF, average value over 4

1063   years, (h, i) evergreen needleleaf forest (ENF), RU-YPF, average value over 4

1064   years, and (j) evergreen broadleaf forest (EBF).

1065 Figure 5. Average and seasonal range of initial slope of the LRC at 16 sites. The

1066 $\alpha_{ave}P_{max}$ value is shown in $mgCO_2 \, (\mu mol \, photon)^{-1}$. The value converted into

1067 $molCO_2 \, (mol \, photon)^{-1}$, which is frequently used in the field of plant physiology,

1068   is shown in parentheses on the vertical axis.

1069 Figure 6. Relationship between CI_{green} and GP2000 for (a) open shrubland (OSH),

1070   savanna (SAV), grassland (GRA), and cropland (CRO) rice paddy (JP-MSE), (b)

1071   deciduous broadleaf forest (DBF) and closed shrubland (CSH) in a permanent

1072   wetland, (c) deciduous needleleaf forest (DNF), (d) evergreen needleleaf forest

1073   (ENF) of *Pinus densiflora* in JP-FJY, (e) ENF except JP-FJY, and (f) evergreen

1074   broadleaf forest (EBF). Solid and dashed lines represent linear regression fitting

1075   results and their one sigma values; asterisks (*) indicate data newly added in this

1076   study.

1077 Figure 7. Cross-validation of linearity in each vegetation group for newly added data.

1078   (a) ES-Agu data for open shrubland (OSH), savanna (SAV), and grassland

1079   (GRA). (b) FR-Hes1 data for deciduous broadleaf forest (DBF) and closed

1080   shrubland (CSH). (c) RU-YLF data for deciduous needleleaf forest (DNF). (d)

1081   Half of the NL-Loo, IT-Lav and RU-YPF data, and (e) FR-Pue data for EBF.

1082 Figure 8. Seasonal variation of flux data in the daily GPP/GPP capacity ratio (blue) and

1083   GPP (pink) for (a) open shrubland (OSH) and savanna (SAV), (b) cropland

1084   (CRO) rice paddy and grassland (GRA), (c) deciduous broadleaf forest (DBF)

1085   and closed shrubland (CSH) in a permanent wetland, (d) deciduous needleleaf

1086   forest (DNF), (e) evergreen needleleaf forest (ENF), and (f) evergreen broadleaf

1087   forest (EBF).

1088 Figure 9. Daily GPP capacity from the CI_{green}, daily GPP of flux data, and MODIS GPP

1089   product for (a) ES-Agu (open shrubland [OSH]), (b) FR-Hes (deciduous

1090   broadleaf forest [DBF]), (c) RU-YLF (deciduous needleleaf forest [DNF]),

1091   average value for 2004−2007, (d) RU-Ypf (evergreen needleleaf forest [ENF]),

1092   average value for 2004−2007, (e) NL-Loo (ENF), (f) IT-Lav (ENF), and (g) FR-

1093   Pue (evergreen broadleaf forest [EBF]). CI_{green} was not available in late June for

1094   FR-Hes and late May for ITLav.

1095 Figure 10. Diurnal variation in the instantaneous GPP capacity from MODIS CI_{green} and

1096   from Flux data, and in Flux GPP for (a1, 2) ES-Agu (open shrubland [OSH]),

1097   (b1, 2) FR-Hes (deciduous broadleaf forest [DBF]), (c1−2) RU-Ylf (deciduous

1098   needleleaf forest [DNF]), (d1, 2) RU-Ypf (evergreen needleleaf forest [ENF]),

1099   (e1, e2) NL-Loo (ENF), (f1−f2) IT-Lav (ENF), and (g1, 2) FR-Pue (evergreen

1100   broadleaf forest [EBF]).

1101 Figure B1. Seasonal changes in GP2000 for (a) open shrubland (OSH), (b) savanna

1102   (SVA), (c) grassland (GRA), (d) cropland (CRO) rice paddy, (e) closed shrubland

1103   (CSH) of permanent wetland, (f) deciduous broadleaf forest (DBF), (g) deciduous

1104   needleleaf forest (DNF), (h, i) evergreen needleleaf forest (ENF), and (j)

1105   evergreen broadleaf forest (EBF).

1106 Figure C1. Relationship between CI_{green} and GP2000 for open shrubland (OSH),

1107   savanna (SAV), grassland (GRA), and cropland (CRO) rice paddy (JP-MSE),

1108   deciduous broadleaf forest (DBF) and closed shrubland (CSH) in a permanent

1109   wetland, deciduous needleleaf forest (DNF), evergreen needleleaf forest (ENF) of

1110   *Pinus densiflora* in JP-FJY, and evergreen broadleaf forest (EBF). The solid line

1111   represents the fitting results from a linear regression, and the dotted lines indicate

1112   the one sigma values for the fitting.

1113   Figure D1. Air temperature and VPD for 16 days from DOY 145 to 161 at the YLF site.

1114

IGBP class	Site ID (This study)	Data year	Name and Country	Location	Annual temp. (°C)	Annual precip.(mm)	Dominant Species	Canopy height(m)	Reference
OSH	ES-Agu*	2007	Balsa Blanca, Spain	36.9406˚N 2.0329˚W	18.0	220	*Machrocloa tenacissima*	1	(López-Ballesteros et al., 2016 López-Ballesteros et al., 2018)
OSH	US-Ses°	2007	Sevilleta shrubland, USA	34.3349˚N 106.7442˚W	13.7	273	*Larrea tridentata, Bouteloua eriopoda*	0.75	(Anderson-Teixeira et al., 2011)
SAV	US-Wjs°	2007	Willard Juniper, Savannah, USA	34.4255˚N 105.862˚W	15.2	361	*Juniperus monosperma, Bouteloua gracilis*	2	(Anderson-Teixeira et al., 2011)
GRA	CA-Let°	2003	Alberta-Mixed Grass, Prairie, Canada	49.709˚N 112.940˚W	5.4	398	*Agropyron dasystachyum A. smithii*	0.317 ± 0.074 (2001-2006)	(Flanagan et al., 2011)
CRO	JP-MSE#	2001-2004	Mase paddy, Japan	36.054˚N 136.054˚E	13.7	1200	rice (*Oryza sativa*)	1.2 (max.)	(Ono et al., 2013)
DBF	FR-Hes*	2007	Hess, France	48.6742˚N 7.0656˚E	9.2	820	Beech (*Fagus sylvatica L.*)	13	(Granier et al., 2008)
DBF	JP-TKY°	2003	Takayama, Japan	36.146˚N 37.423˚E	6.4	2293.5	*Betula ermanii Quercus crispula*	15-20	(Saigusa et al., 2002) (Hirata, et al., 2008)
CSH (WET)	US-Los*	2007	Lost Creek, USA	46.0827˚N 89.9792˚W	4.1	828	Alder (*Alnus incana*) Willow (*Salix*)	2	(US-Los; Sulman et al., 2009)
DNF	RU-YLF*	2004-2007	Spasskaya Pad, Yakutsk, Russia	62.255˚N 129.241389˚E	-10.0 (1961-1990)	236.9 (1961-1990)	Dahurica larch (*Larix cajanderi*)	18	(Ohta et al., 2008)
DNF	JP-TMK°	2003	Tomakomai, Japan	42.737˚N 141.519˚E	6.2	1043	Japanese larch (*Larix kaempferi*)	15	(Hirata, et al., 2007, 2008)
ENF	NL-Loo*	2007	Loobos, Netherlands	52.1679˚N 5.7440˚E	9.8	786	Scots pine (*Pinus sylverstris*)	15.1 (1977)	(Dolman et al., 2002)
ENF	IT-Lav*	2007	Lavarone, Italy	45.9553˚N 11.2812˚E	7.0	1150	Fir *Abies alba* (70%)	33-36	(Marcolla et al., 2003)
ENF	RU-YPF*	2004-2007	Spasskaya Pad, Yakutsk, Russia	62.241389˚N 129.650556˚E	-10.0 (1961-1990)	236.9 (1961-1990)	Pine (*Pinus sylvestris*)	10	(Matsumoto et al., 2008)

ENF	JP-FJY∘	2003	Fujiyoshida, Japan	35.454˚N 138.762˚E	10.1	1483	Japanese red pine *(Pinus densiflora)*	20	(Mizoguchi et al., 2012) (Hirata, et al., 2008)
EBF	FR-Pue*	2007	Puechabon, France	43.7414˚N 3.5958˚E	10.4	1230	Holm oak *(Quercus ilex L.)*	6	(Soudani et al., 2014)
EBF	TH-SHR∘	2003	Sakaerat, Thailand	14.492˚N 101.916˚E	24.1	1200-1300	*Hopea ferrea pierre*	35	(Aguilos et al., 2007) (Hirata, et al., 2008)

Vegetation types (IGBP class) (IGBP class)	GP2000			No. of data	$GP2000 = aCI_{green} + b$		RMSE	R^2	p
	min.	max.	ave.		a	b			
Open shrubland (OSH)									
Savanna (SVA)	0.01	1.57	0.36	123	0.4±0.01	-0.28 ±0.02	0.11	0.94	<0.001
Grasslands (GRA)									
Croplands (CRO)									
Deciduous broadleaf forest (DBF)	0.02	1.32	0.58	49	0.17±0.01	-0.34±0.07	0.19	0.81	<0.001
Closed shrubland (CSH)									
Deciduous needleleaf forest (DNF)	0.16	1.66	0.52	45	0.24±0.01	-0.31±0.05	0.14	0.87	<0.001
Red pine of JP-FJY (ENF)	0.51	1.26	0.96	9	0.18±0.04	0.15±0.18	0.11	0.76	0.002

| Evergreen needleleaf forest (ENF) | 0.21 | 1.08 | 0.63 | 65 | 0.15±0.02 | 0.03±0.07 | 0.17 | 0.54 | <0.001 |
| Evergreen broadleaf forest (EBF) | 0.32 | 1.37 | 0.73 | 27 | 0.16±0.03 | -0.09±0.17 | 0.18 | 0.51 | <0.001 |

Highlights

- The light-response-curve parameters were assessed for nine vegetation types.

- GP2000 had a linear relationship with CI_{green}.

- The linear relationships were quantified for nine vegetation types.

- Diurnal GPP capacity could be the baseline for the diurnal depression of GPP.

Declaration of interests

☒ The authors declare that they have no known competing financial interests or personal relationships that could have appeared to influence the work reported in this paper.

☐ The authors declare the following financial interests/personal relationships which may be considered as potential competing interests: